Dipole-dipole interaction in cavity QED: The weak-coupling, nondegenerate regime

M. Donaire,[1,2,*] J. M. Muñoz-Castañeda,[3] and L. M. Nieto[1]

[1]*Departamento de Física Teórica, Atómica y Óptica and IMUVA, Universidad de Valladolid, Paseo Belén 7, 47011 Valladolid, Spain*

[2]*Facultad de Educación de Palencia, Campus La Yutera, Universidad de Valladolid, Avd. Madrid, 44, 34004 Palencia, Spain*

[3]*Departamento de Física, ETSIAE, Universidad Politécnica de Madrid, 28049 Madrid, Spain*

(Received 31 January 2017; revised manuscript received 7 September 2017; published 24 October 2017)

We compute the energies of the interaction between two atoms placed in the middle of a perfectly reflecting planar cavity, in the weak-coupling nondegenerate regime. Both inhibition and enhancement of the interactions can be obtained by varying the size of the cavity. We derive exact expressions for the dyadic Green's function of the cavity field which mediates the interactions and apply time-dependent quantum perturbation theory in the adiabatic approximation. We provide explicit expressions for the van der Waals potentials of two polarizable atomic dipoles and the electrostatic potential of two induced dipoles. We compute the van der Waals potentials in three different scenarios: two atoms in their ground states, two atoms excited, and two dissimilar atoms with one of them excited. In addition, we calculate the phase-shift rate of the two-atom wave function in each case. The effect of the two-dimensional confinement of the electromagnetic field on the dipole-dipole interactions is analyzed. This effect depends on the atomic polarization. For dipole moments oriented parallel to the cavity plates, both the electrostatic and the van der Waals interactions are exponentially suppressed for values of the cavity width much less than the interatomic distance, whereas for values of the width close to the interatomic distance, the strength of both interactions is higher than their values in the absence of cavity. For dipole moments perpendicular to the plates, the strength of the van der Waals interaction decreases for values of the cavity width close to the interatomic distance, while it increases for values of the width much less than the interatomic distance with respect to its strength in the absence of cavity. We illustrate these effects by computing the dipole-dipole interactions between two alkali atoms in circular Rydberg states.

DOI: 10.1103/PhysRevA.96.042714

I. INTRODUCTION

Modifying the interaction of atoms with the electromagnetic (EM) field by means of a cavity is at the origin of cavity QED [1,2]. In the first place, a perfectly reflecting cavity reduces the density of EM states accessible to the spontaneous emission of a single atom. This results in an enhancement of the atomic lifetime as well as in a shift of the atomic levels. On the other hand, the strong coupling between the cavity modes and the atomic charges drives the coherent exchange of excitations between the atom and the cavity field [3]. For the case of a perfectly reflecting planar cavity, the atomic level shifts [4–8] and the modified lifetimes of an excited atom have been well studied theoretically [9–11] and measured experimentally [1,2,12]. Ultimately, these effects make possible the coherent manipulation of quantum states, the entanglement between separated quantum systems [13,14], and the storage of quantum information [15–17].

Considering the cavity as a macroscopic system hardly affected by the presence of the atoms inside, the interaction of the free EM field with the cavity plates can be integrated out in an effective Hamiltonian. The resultant EM interactions of the atoms are commonly referred to as cavity-assisted interactions [13,18,19]. This is a good approximation, as long as the absorption and emission spectra of the atoms and the cavity material do not overlap, and as long as the time resolution of observation is much larger than the time of flight of photons from the atoms to the cavity plates. Under these conditions, transient transitions average out and the effective cavity-assisted interactions become stationary. The net result is that photon states get *dressed* by multiple-scattering processes with the cavity plates, and so does the photon propagator. It is the modes of the dressed EM field which are commonly referred to as cavity modes of the cavity field.

On the other hand, dispersion forces between neutral atoms and between atoms and macroscopic surfaces are the result of the coupling of the quantum fluctuations of the EM field, the atomic charges, and the surface currents [9,19]. The interaction between an atom and a macroscopic surface is known as *Casimir-Polder interaction* [19–23], whereas the interaction between two neutral atoms is known generally as *van der Waals interaction* [9,19,24–30]—referred to as *London interaction* for interatomic distances smaller than the resonant wavelength [31]. In this article we combine both kinds of interactions in a three-body problem. We address the cavity-assisted dipole-dipole interaction between two atoms placed in the middle of a perfectly reflecting cavity, at zero temperature, see Fig. 1. This is a common setup in the generation of quantum entanglement with Rydberg atoms [13,32], also in the absence of a cavity [33]. In particular, we study the modification of the atom-atom interactions varying the size of the cavity. We compute several quantities of interest in the weak-coupling, nondegenerate regime. These are the van der Waals (vdW) potentials for the case that both atoms are in their ground states, for the case that both atoms are excited, and for the case that one atom is excited while the other, of a different kind, is in its ground state. In addition, we calculate the electrostatic potential between two induced atomic dipoles. We calculate in

*On leave from Laboratoire Kastler Brossel, UPMC-Sorbonnes Universités, CNRS, ENS-PSL Research University, Collège de France; manuel.donaire@uva.es; mad37ster@gmail.com

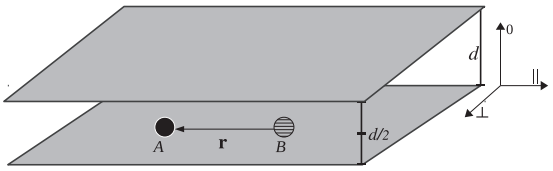

FIG. 1. Sketch of the setup of the problem.

each case the corresponding phase-shift rate of the two-atom wave function.

Physically, the vdW and electrostatic potentials can be observed through the forces experienced by each atom when placed inside harmonic traps, which are proportional to the displacements of the atoms with respect to their equilibrium positions in the absence of interaction. On the other hand, the phase shift of the two-atom wave function can be observed using atom interferometry. For instance, it is the shift that is observed in the binary interaction of Rydberg atoms through the measurement of population probabilities [14,34].

Concerning our approach, we apply time-dependent quantum perturbation theory, up to fourth order, in the electric dipole approximation [35]. Except for the degenerate interaction addressed at the end of Sec. V, all the calculations are carried out in the perturbative nondegenerate regime, where the energy difference between the intermediate and initial atomic states is much greater than the interaction energy and the atom-cavity coupling is weak. In particular, the latter implies that we cannot restrict ourselves to the one-cavity mode approximation of the Jaynes-Cummings Hamiltonian [2]. For the case of the interaction between excited atoms, the excitation is assumed adiabatic with respect to the detuning between the atomic species, which is a situation commonly encountered in experiments.

The main achievements of this work are, in the first place, the computation of the Green function for the cavity field which mediates the interaction between two atomic dipoles placed in the middle of the cavity. The effects of the two-dimensional confinement of the EM field are revealed. Second, we find out explicit expressions for the resonant components of the vdW potentials of each atom when excited. The difference between each atom's potentials as well as their discrepancy with the phase-shift rate of the wave function are exposed.

The paper is organized as follows. In Sec. II we describe the setup of the problem and compute the dyadic Green's function of the cavity field. In Sec. III we calculate the vdW potentials and the phase shifts on two-atom systems in the nondegenerate regime. In Sec. IV we compute the electrostatic potential of two induced dipoles. All the formulas derived in the previous sections are applied in Sec. V to the calculation of the dipole-dipole interactions between two circular Rydberg atoms in a cavity. We summarize the conclusions in Sec. VI.

II. GREEN'S DYADIC OF THE CAVITY FIELD

We aim at computing the cavity-assisted dipole-dipole interactions between two atoms, A and B, placed in the middle of a perfectly reflecting planar cavity of thickness d and separated by a distance $\mathbf{r}$ along an axis parallel to the cavity plates (see Fig. 1). These interactions are mediated by virtual photons created and annihilated at the position of each atom. Therefore the relevant quantity to be computed is the Green function of the cavity field that the atomic dipoles induce at the position of each other. To this end, we use the effective semiclassical approach outlined in the Introduction. The plates of the cavity are treated as passive and semiclassical objects which reflect photons with no losses. The free Hamiltonian of the atoms and the EM cavity field is $H_0 = H_A + H_B + H_{EM}$, with

$$\begin{aligned} H_A &= \sum_i \hbar\omega_i^A |A_i\rangle\langle A_i|, \quad H_B = \sum_i \hbar\omega_i^B |B_i\rangle\langle B_i|, \\ H_{EM} &= \frac{\epsilon_0}{2}\int d^3R\,[|\mathbf{E}(\mathbf{R})|^2 + c^2|\mathbf{B}(\mathbf{R})|^2] \\ &= \sum_{\mathbf{k},\vec{\epsilon}} \hbar\omega(a^\dagger_{\mathbf{k},\vec{\epsilon}}\, a_{\mathbf{k},\vec{\epsilon}} + 1/2). \end{aligned} \tag{1}$$

Here, $|A_i\rangle$, $|B_i\rangle$ denote the ith states of atoms A, B, with energies $\hbar\omega_i^A$ and $\hbar\omega_i^B$, respectively. The operators $a^\dagger_{\mathbf{k},\vec{\epsilon}}$ and $a_{\mathbf{k},\vec{\epsilon}}$ are the creation and annihilation operators of photons of frequency $\omega = ck$, momentum $\hbar\mathbf{k}$, and polarization vector $\vec{\epsilon}$, respectively, in terms of which the electric field operator reads

$$\begin{aligned} \mathbf{E}(\mathbf{R}) &= \sum_{\mathbf{k}} \mathbf{E}^{(-)}_{\mathbf{k}}(\mathbf{R}) + \mathbf{E}^{(+)}_{\mathbf{k}}(\mathbf{R}) \\ &= i\sum_{\mathbf{k},\vec{\epsilon}} \sqrt{\frac{\hbar ck}{2\mathcal{V}\epsilon_0}}[\vec{\epsilon}\, a_{\mathbf{k}} e^{i\mathbf{k}\cdot\mathbf{R}} - \vec{\epsilon}^{\,*} a^\dagger_{\mathbf{k}} e^{-i\mathbf{k}\cdot\mathbf{R}}], \end{aligned} \tag{2}$$

with $\mathcal{V}$ being a volume of quantization. The magnetic field operator relates to $\mathbf{E}(\mathbf{R})$ through Maxwell's equation, $\boldsymbol{\nabla}\times\mathbf{E}(\mathbf{R}) = -\partial\mathbf{B}(\mathbf{R})/\partial t$. Our semiclassical approximation with regard to the interaction between the EM field and the cavity plates consists of assuming that the virtual photons created at the location of one of the atoms reflect off the plates any number of times before being absorbed either by itself or by the other atom. In each reflection process the dynamical excitation of the plates is discarded, and so is the time of flight of photons between any pair of scattering processes. Under these conditions, the intermediate photonic states and the EM vacuum can be considered as dressed by multiple reflection processes with the cavity plates [7,23]. Equivalently, the dressing can be assigned to the electric field operator within the framework of macroscopic QED [18,19]. The net result is the effective discretization of the modes of the EM field within the cavity. Mathematically, this is achieved by taking the cavity volume as the volume of quantization in Eq. (2), $\mathcal{V} = \mathcal{V}_{\mathrm{Cav}}$, or equivalently, by imposing ideal boundary conditions in Maxwell's equations for the electric and magnetic field. Those conditions consist in the components of the electric field parallel to the plates and of the associated magnetic field perpendicular to the plates going to zero [19,36,37]. Alternatively, we can write Maxwell's equation for the dyadic Green's function $\mathbb{G}$ of the electric field induced at a point $\mathbf{R}'$ by a nonpolarizable electric dipole of frequency $\omega = ck$ placed at $\mathbf{R}$,

$$[\omega^2\mathbb{I} - \boldsymbol{\nabla}\times\boldsymbol{\nabla}\times]\mathbb{G}(\mathbf{R}';\mathbf{R};k) = \delta^{(3)}(\mathbf{R}'-\mathbf{R})\mathbb{I}, \tag{3}$$

and impose the boundary conditions at the plates [37],

$$\begin{aligned}\hat{\mathbf{n}}\times\mathbb{G}(\mathbf{R}';\mathbf{R};k)|_{\mathbf{R}'\text{on the plates}}&=\mathbf{0},\\(\hat{\mathbf{n}}\cdot\nabla)\cdot[\mathbb{G}(\mathbf{R}';\mathbf{R};k)-k^2\delta^{(3)}(\mathbf{R}'-\mathbf{R})]|_{\mathbf{R}'\text{on the plates}}&=\mathbf{0},\end{aligned}\tag{4}$$

where $\hat{\mathbf{n}}$ is a unitary vector, outward-pointing and orthogonal to the plates. By doing so, the resultant components of the dyadic Green's function for the electric field induced at a point $(\mathbf{r},d/2)$ by a nonpolarizable electric dipole of frequency $\omega=ck$ placed at $(\mathbf{0},d/2)$ are [37]

$$G_{\parallel\parallel}(\mathbf{r},d/2;k)=\int\frac{d^2q}{2(2\pi)^2}e^{i\mathbf{q}\cdot\mathbf{r}}\frac{q_\parallel^2-k^2}{k^2\rho\sin\rho d}(1-\cos\rho d),\tag{5}$$

$$G_{\perp\perp}(\mathbf{r},d/2;k)=\int\frac{d^2q}{2(2\pi)^2}e^{i\mathbf{q}\cdot\mathbf{r}}\frac{q_\perp^2-k^2}{k^2\rho\sin\rho d}(1-\cos\rho d),\tag{6}$$

$$G_{00}(\mathbf{r},d/2;k)=\int\frac{d^2q}{2(2\pi)^2}e^{i\mathbf{q}\cdot\mathbf{r}}\frac{q^2}{k^2\rho\sin\rho d}(1+\cos\rho d),\tag{7}$$

where $\mathbf{q}$ is a two-dimensional reciprocal vector parallel to the plates and $\rho\equiv\sqrt{k^2-q^2}$. The quantization axis is taken perpendicular to the plates, which is denoted by the index 0, while the indices $\parallel$ and $\perp$ refer to the axes parallel to the plates, which are parallel and perpendicular to $\mathbf{r}$, respectively (cf. Fig. 1). The off-diagonal components are all null.

The photons mediating the interactions between the two atoms are created at the position of the atoms by the EM field operators which enter the interaction Hamiltonian, W. It reads, in the electric dipole approximation, $W=W_A+W_B$, with $W_{A,B}=-\mathbf{d}_{A,B}\cdot\mathbf{E}(\mathbf{R}_{A,B})$. Here $\mathbf{d}_{A,B}$ are the electric dipole moment operators of each atom, $\mathbf{E}$ is the electric field operator, and $\mathbf{R}_{A,B}$ are the classical position vectors of the atomic centers of mass, with $\mathbf{r}=\mathbf{R}_A-\mathbf{R}_B$. W is considered as a perturbation to H_0. Higher multipole orders in the interaction would be relevant for values of r or d in the order of a few times the atomic radius [36]. Throughout this work we restrict ourselves to values of r and d at least an order of magnitude larger than the atomic radii, such that the electric dipole approximation suffices.

According to the fluctuation-dissipation theorem, the quadratic fluctuations of the electric field in the dressed vacuum, $|\tilde{0}_\gamma\rangle$, read at zero temperature:

$$\langle\tilde{0}_\gamma|\mathbf{E}(\mathbf{0},d/2;k)\mathbf{E}^\dagger(\mathbf{r},d/2;k)|\tilde{0}_\gamma\rangle=\frac{-\hbar k^2}{\pi\epsilon_0}\mathrm{Im}[\mathbb{G}(\mathbf{r},d/2;k)].\tag{8}$$

It will be useful in the calculations to use the identity $\sin^{-1}\rho d=-2i(1+e^{i\rho d})\sum_{m=1}^{\infty}e^{i\rho md}$ in order to write $\mathbb{G}$ as an infinite power series. In doing so, it is possible to ascribe a simple physical meaning to each term of the resultant series. That is, the term of order m, say $\mathbb{G}^{(m)}\sim e^{i\,md\rho}$, accounts for the contribution of m reflections off the plates. In the following, we will use either formulation according to its mathematical manageability. Lastly, it is also useful to write the components of $\mathbb{G}$ in the spherical basis, with components $\{0,+,-\}$, in order to trace the polarization of the photons which mediate the corresponding atomic transitions, $\{\pi,\sigma^-,\sigma_+\}$, respectively. The change of basis yields the following relationships: $G_{+-}=G_{-+}=(G_{\parallel\parallel}+G_{\perp\perp})/2$, $G_{++}=G_{--}=(G_{\parallel\parallel}-G_{\perp\perp})/2$.

The imaginary parts of $G_{\parallel\parallel}$, $G_{\perp\perp}$, and G_{00} derive from the poles of Eqs. (5), (6), and (7), respectively:

$$\mathrm{Im}[G_{\parallel\parallel}(\mathbf{r},d/2;k)]=\sum_{n=1}^{\mathrm{Int}(\frac{kd}{\pi})}\frac{(-1)^n-1}{4dk^2}\left[\frac{n^2\pi^2}{d^2}J_0(r\sqrt{k^2-n^2\pi^2/d^2})+\frac{\sqrt{k^2-n^2\pi^2/d^2}}{r}J_1(r\sqrt{k^2-n^2\pi^2/d^2})\right],\tag{9}$$

$$\mathrm{Im}[G_{\perp\perp}(\mathbf{r},d/2;k)]=\sum_{n=1}^{\mathrm{Int}(\frac{kd}{\pi})}\frac{(-1)^n-1}{4dk^2}\left[k^2J_0(r\sqrt{k^2-n^2\pi^2/d^2})-\frac{\sqrt{k^2-n^2\pi^2/d^2}}{r}J_1(r\sqrt{k^2-n^2\pi^2/d^2})\right],\tag{10}$$

$$\mathrm{Im}[G_{00}(\mathbf{r},d/2;k)]=\frac{-1}{4d}J_0(kr)-\frac{1}{2k^2d}\sum_{n=1}^{\mathrm{Int}(\frac{kd}{2\pi})}[k^2-4\pi^2n^2/d^2]\,J_0(r\sqrt{k^2-4n^2\pi^2/d^2}),\tag{11}$$

where J_0 and J_1 are the Bessel functions of the first kind of orders 0 and 1, respectively. As for the real parts of $\mathbb{G}$, making use of the Kramers-Kronig relationship, $k^2\mathrm{Re}[\mathbb{G}(k)]=\frac{2}{\pi}\int_0^\infty dk'k'^3\mathrm{Im}[\mathbb{G}(k')]/(k'^2-k^2)$, we obtain

$$\begin{aligned}\mathrm{Re}[G_{\parallel\parallel}(\mathbf{r},d/2;k)]=&-\sum_{n=1}^{\mathrm{Int}(\frac{kd}{\pi})}\frac{(-1)^n-1}{4dk^2}\left[\frac{n^2\pi^2}{d^2}Y_0(r\sqrt{k^2-n^2\pi^2/d^2})+\frac{\sqrt{k^2-n^2\pi^2/d^2}}{r}Y_1(r\sqrt{k^2-n^2\pi^2/d^2})\right]\\&+\sum_{n=\mathrm{Int}(\frac{kd}{\pi})+1}^{\infty}\frac{(-1)^n-1}{2\pi dk^2}\left[\frac{n^2\pi^2}{d^2}K_0(r\sqrt{n^2\pi^2/d^2-k^2})+\frac{\sqrt{n^2\pi^2/d^2-k^2}}{r}K_1(r\sqrt{n^2\pi^2/d^2-k^2})\right],\end{aligned}\tag{12}$$

$$\mathrm{Re}[G_{\perp\perp}(\mathbf{r},d/2;k)] = -\sum_{n=1}^{\mathrm{Int}(\frac{kd}{\pi})}\frac{(-1)^n-1}{4dk^2}\left[k^2Y_0(r\sqrt{k^2-n^2\pi^2/d^2})-\frac{\sqrt{k^2-n^2\pi^2/d^2}}{r}Y_1(r\sqrt{k^2-n^2\pi^2/d^2})\right]$$
$$+\sum_{n=\mathrm{Int}(\frac{kd}{\pi})+1}^{\infty}\frac{(-1)^n-1}{2\pi dk^2}\left[k^2K_0(r\sqrt{n^2\pi^2/d^2-k^2})-\frac{\sqrt{n^2\pi^2/d^2-k^2}}{r}K_1(r\sqrt{n^2\pi^2/d^2-k^2})\right], \tag{13}$$

$$\mathrm{Re}[G_{00}(\mathbf{r},d/2;k)] = \frac{1}{4d}Y_0(kr)+\frac{1}{2k^2d}\sum_{n=1}^{\mathrm{Int}(\frac{kd}{2\pi})}[k^2-4\pi^2n^2/d^2]\,Y_0(r\sqrt{k^2-4n^2\pi^2/d^2})-\frac{1}{\pi k^2d}\sum_{n=\mathrm{Int}(\frac{kd}{2\pi})+1}^{\infty}[k^2-4\pi^2n^2/d^2]$$
$$\times K_0(r\sqrt{4n^2\pi^2/d^2-k^2}), \tag{14}$$

where $Y_{0,1}$ and $K_{0,1}$ are the Bessel functions (Y) and modified Bessel functions (K) of the second kind, of orders 0 and 1, respectively.

Alternatively, the above expressions can be written as a series in powers of the number of reflections off the plates,

$$G_{\parallel\parallel}(\mathbf{r},d/2;k) = \frac{-e^{ikr}}{4\pi k^2}\left[\frac{2}{r^3}-\frac{2ik}{r^2}\right]-\sum_{n=1}^{\infty}(-1)^n\frac{ik}{2\pi}\int_0^1 d\zeta\, e^{i\zeta knd}\left[\frac{1+\zeta^2}{kr\sqrt{1-\zeta^2}}J_1(kr\sqrt{1-\zeta^2})-\zeta^2J_2(kr\sqrt{1-\zeta^2})\right]$$
$$-\sum_{n=1}^{\infty}(-1)^n\frac{k}{2\pi}\int_0^{\infty}d\zeta\, e^{-\zeta knd}\left[\frac{1-\zeta^2}{kr\sqrt{1+\zeta^2}}J_1(kr\sqrt{1+\zeta^2})+\zeta^2J_2(kr\sqrt{1+\zeta^2})\right], \tag{15}$$

$$G_{\perp\perp}(\mathbf{r},d/2;k) = \frac{-e^{ikr}}{4\pi k^2}\left[\frac{-1}{r^3}+\frac{ik}{r^2}+\frac{k^2}{r}\right]-\sum_{n=1}^{\infty}(-1)^n\frac{ik}{2\pi}\int_0^1 d\zeta\, e^{i\zeta knd}\left[\frac{1+\zeta^2}{kr\sqrt{1-\zeta^2}}J_1(kr\sqrt{1-\zeta^2})-J_2(kr\sqrt{1-\zeta^2})\right]$$
$$-\sum_{n=1}^{\infty}(-1)^n\frac{k}{2\pi}\int_0^{\infty}d\zeta\, e^{-\zeta knd}\left[\frac{1-\zeta^2}{kr\sqrt{1+\zeta^2}}J_1(kr\sqrt{1+\zeta^2})-J_2(kr\sqrt{1+\zeta^2})\right], \tag{16}$$

$$G_{00}(\mathbf{r},d/2;k) = \frac{-e^{ikr}}{4\pi k^2}\left[\frac{-1}{r^3}+\frac{ik}{r^2}+\frac{k^2}{r}\right]-\sum_{n=1}^{\infty}(-1)^n\frac{ik}{2\pi}\int_0^1 d\zeta\, e^{i\zeta knd}(1-\zeta^2)J_0(kr\sqrt{1-\zeta^2})$$
$$-\sum_{n=1}^{\infty}(-1)^n\frac{k}{2\pi}\int_0^{\infty}d\zeta\, e^{-\zeta knd}(1+\zeta^2)J_0(kr\sqrt{1+\zeta^2}), \tag{17}$$

where the dimensionless variable of integration ζ is such that $k\sqrt{1-\zeta^2}$ is the norm of the two-dimensional reciprocal vector parallel to the plates. In Appendix A we give the expressions of the Green function components in the spherical basis in the asymptotic limits $d \gg r,k^{-1}$ [i.e., three-dimensional (3D) limit] and $d \ll r,k^{-1}$ [i.e., two-dimensional (2D) limit].

III. VAN DER WAALS POTENTIALS

At leading order in time-dependent perturbation theory, i.e., order four in W, 24 processes contribute to the vdW potentials of each atom in which two photons are exchanged between the two atoms in all possible orders in time, two terms for each of the diagrams in Figs. 2 and 3 [28,38,39]. In terms of the vdW potentials, $\langle W_{A,B}/2\rangle$, the forces on each atom are $\mathbf{F}_{A,B} = \mp\boldsymbol{\nabla}_{\mathbf{r}}\langle W_{A,B}/2\rangle$, respectively, with $\mathbf{r} = \mathbf{R}_A - \mathbf{R}_B$ [38]. In every case, i.e., either for ground- or for excited-state atoms, virtual transitions between atomic levels are accompanied by the exchange of off-resonant photons of frequency $\omega \lesssim c/r$. Their contribution to the vdW potentials are referred to as off-resonant vdW potentials. In addition, for the case that one or both atoms are excited, transitions to lower-energy atomic levels proceed through the exchange of photons which resonate with the transitions. Their contribution to the vdW potentials are referred to as resonant vdW potentials [18,23]. Interestingly, while the off-resonant potentials of each atom are equivalent, their resonant potentials differ [38,39].

For the sake of illustration we give below the expression of diagram (1) in Fig. 2,

$$\sum_{l,j}\frac{1}{\hbar^3}\int_0^{\infty}\frac{\mathcal{V}k^2dk}{(2\pi)^3}\int_0^{\infty}\frac{\mathcal{V}k'^2dk'}{(2\pi)^3}\int_0^{4\pi}d\Omega\int_0^{4\pi}d\Omega'\Big\{\Big[i\,\langle a,b,\tilde{0}_\gamma|e^{i(\omega_a+\omega_b)T}|a,b,\tilde{0}_\gamma\rangle\int_{-\infty}^{T}dt\int_{-\infty}^{t}dt'\int_{-\infty}^{t'}dt''$$
$$\times e^{\eta(t+t'+t'')}\langle a,b,\tilde{0}_\gamma|\mathbf{d}_A\cdot\mathbf{E}^{(-)}_{\mathbf{k}'}(\mathbf{R}_A)|l,b,\tilde{1}_{\mathbf{k}'}\rangle e^{-i(\omega'+\omega_l+\omega_b)(T-t)}\langle l,b,\tilde{1}_{\mathbf{k}'}|\mathbf{d}_B\cdot\mathbf{E}^{(+)}_{\mathbf{k}'}(\mathbf{R}_B)|l,j,\tilde{0}_\gamma\rangle$$
$$\times e^{-i(\omega_l+\omega_j)(t-t')}\langle l,j,\tilde{0}_\gamma|\mathbf{d}_B\cdot\mathbf{E}^{(-)}_{\mathbf{k}}(\mathbf{R}_B)|l,b,\tilde{1}_{\mathbf{k}}\rangle e^{-i(\omega+\omega_l+\omega_b)(t'-t'')}\langle l,b,\tilde{1}_{\mathbf{k}}|\mathbf{d}_A\cdot\mathbf{E}^{(+)}_{\mathbf{k}}(\mathbf{R}_A)|a,b,\tilde{0}_\gamma\rangle e^{-i(\omega_a+\omega_b)t''}\Big]$$
$$+[k\leftrightarrow k']^{\dagger}\Big\},\quad \eta\to 0^+, \tag{18}$$

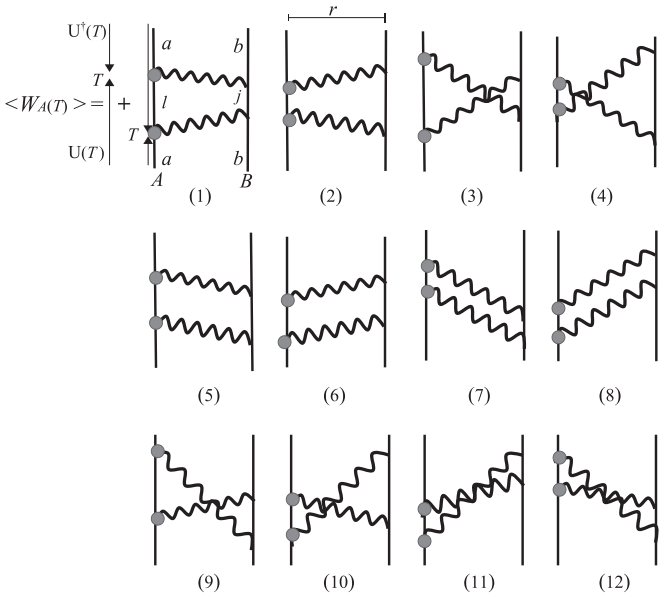

FIG. 2. Diagrammatic representation of the 24 terms which contribute to $\langle W_A(T)\rangle$, two for each of the 12 diagrams. Thick straight lines stand for propagators of atomic states, while wavy lines stand for photon propagators. In diagram (1), the initial states a, b, and the generic intermediate states of each atom l, j are indicated. Although not shown, the same states appear in the rest of the diagrams in analogous sites. The atoms A and B are separated by a distance r along the horizontal direction, whereas time runs along the vertical. The gray circles on the left of each diagram stand for the insertion of the Schrödinger operator W_A whose expectation value is computed. Each diagram contributes with two terms, one from each of the operators W_A inserted. They are sandwiched between two time propagators, $\mathrm{U}(T)$ and $\mathrm{U}^\dagger(T)$ (depicted by vertical arrows), which evolve the initial state $|a,b,\tilde{0}_\gamma\rangle$ towards the observation time at which W_A applies.

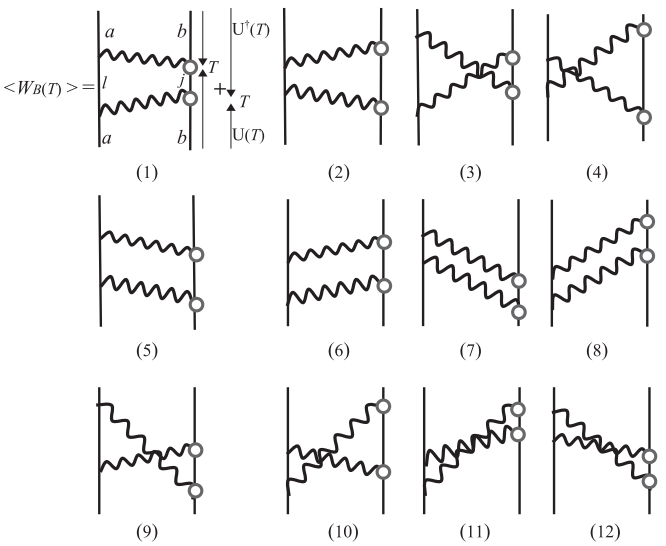

FIG. 3. Diagrammatic representation of the 24 terms which contribute to $\langle W_B(T)\rangle$, two for each of the 12 diagrams. Thick straight lines stand for propagators of atomic states, while wavy lines stand for photon propagators. In diagram (1), the initial states a, b and the generic intermediate states of each atom l, j are indicated. Although not shown, the same states appear in the rest of diagrams in analogous sites. The atoms A and B are separated by a distance r along the horizontal direction, whereas time runs along the vertical. The white circles on the right of each diagram stand for the insertion of the Schrödinger operator W_B whose expectation value is to be computed. Each diagram contributes with two terms, one from each of the operators W_B inserted. They are sandwiched between two time propagators, $\mathrm{U}(T)$ and $\mathrm{U}^\dagger(T)$ (depicted by vertical arrows), which evolve the initial state $|a,b,\tilde{0}_\gamma\rangle$ towards the observation time at which W_B applies.

where $|a,b,\tilde{0}_\gamma\rangle$ is the quasistationary (*initial*) two-atom–zero-photon state, $|l\rangle$ and $|j\rangle$ are intermediate atomic states of the atoms A and B, respectively, $|\tilde{1}_{\mathbf{k}}\rangle$ is a one-cavity photon state of momentum $\mathbf{k}$ and frequency $\omega = ck$, the complex time exponentials are the result of the application of the free time-evolution operator $\mathrm{U}_0(t) = e^{-i\hbar^{-1}H_0 t}$ between the interaction vertices $W_{A,B}$, and the real time exponential $e^{\eta(t+t'+t'')}$ takes care of the adiabatic approximation. After integrating in time and solid angles, and using the fluctuation-dissipation relation of Eq. (8), one arrives at

$$\sum_{l,j}\frac{8\alpha_f c^3}{\pi\epsilon_0 e^2}\frac{d_{la}^m d_{jb}^n d_{bj}^s d_{al}^p}{\omega_a+\omega_b-\omega_l-\omega_j}\mathrm{Re}\int_0^\infty dk\,\frac{k^2\mathrm{Im}G_{mn}(\mathbf{r},k)}{\omega-\omega_a+\omega_l-i\eta}$$
$$\times\int_0^\infty dk'\,\frac{k'^2\mathrm{Im}G_{sp}(\mathbf{r},k')}{\omega'-\omega_a+\omega_l-i\eta},\quad \eta\to 0^+, \tag{19}$$

where α_f is the fine-structure constant and summation over repeated tensor indices is implicit. Generally, the rest of the diagrams yield integrands analogous to the one in Eq. (19), which may contain poles at the transition frequencies. Those poles are slightly shifted along the imaginary axis as a consequence of the adiabaticity parameter $\eta\to 0^+$. When performing the integral over k and k' in the complex plane along the quarter-circle of infinite radius in the first quadrant, one can separate the integral along the positive imaginary axis from the sum over residues. The former is part of the off-resonant vdW interaction, while the latter is part of the resonant vdW interaction [19,23,40,41]. We compile in Appendix B the equations of the contributions of some diagrams to the resonant components of the vdW potentials and phase shifts.

A. Off-resonant van der Waals potentials and off-resonant phase-shift rate

The off-resonant component of the vdW potentials is present in the interaction between any pair of atoms, regardless of whether they are in excited or ground states. It includes upwards and downwards virtual transitions to any intermediate atomic levels in the 12 diagrams of Figs. 2 and 3. In the calculation, the imaginary shifts of the poles in equations analogous to Eq. (19), with $\eta\to 0^+$ in the adiabatic approximation, play no role, and the off-resonant potentials can be also computed within the framework of stationary perturbation theory [18,19,23–25]. This explains also the fact that the off-resonant potentials of each atom coincide, $\langle W_A/2\rangle_{\mathrm{off}} = \langle W_B/2\rangle_{\mathrm{off}}$, and so does the associated phase-shift rate of the two-atom wave function, $\delta\mathcal{E}_{\mathrm{off}} = \langle W_{A,B}/2\rangle_{\mathrm{off}}$ [38].

Let us denote by a and b the states of the atoms A and B, respectively. By adding up equations analogous to that in

Eq. (19) coming from the 12 diagrams of Figs. 2, 3, or 5, one obtains the following integral along imaginary frequencies [18,24,25], $k = iu$:

$$\langle W_{A,B}/2\rangle_{\rm off} = \frac{-2}{\pi\hbar\epsilon_0^2 c^3}\sum_{i,j}\int_0^\infty du\,\frac{u^4\omega_{ia}\omega_{jb}}{(u^2+k_{ia}^2)(u^2+k_{jb}^2)} \times \mathbf{d}_{ai}\cdot\mathbb{G}(\mathbf{r};iu)\cdot\mathbf{d}_{jb}\,\mathbf{d}_{bj}\cdot\mathbb{G}(\mathbf{r};iu)\cdot\mathbf{d}_{ia} = \delta\mathcal{E}_{\rm off}, \tag{20}$$

with $\omega_{ia} = \omega_i - \omega_a$, $k_{ia} = \omega_{ia}/c$, $\omega_{jb} = \omega_j - \omega_b$, $k_{jb} = \omega_{jb}/c$, $\mathbf{d}_{ai} = \langle a|\mathbf{d}_A|i\rangle$, and $\mathbf{d}_{bj} = \langle b|\mathbf{d}_B|j\rangle$. As it stands, it suffices to substitute the expressions of the Green function components in order to calculate the off-resonant vdW potential for any particular case. Evaluating Eqs. (15)–(17) at imaginary frequencies and performing the summation over any number of reflections, we find in the spherical basis,

$$G_{+-}(\mathbf{r};iu) = \frac{e^{-ur}}{8\pi u^2}[1/r^3 + u/r^2 - u^2/r] + \int_1^\infty \frac{d\zeta}{4\pi}\frac{e^{u\zeta d}-1}{e^{2u\zeta d}-1}u(1+\zeta^2)J_0(ur\sqrt{\zeta^2-1}), \tag{21}$$

$$G_{++}(\mathbf{r};iu) = \frac{e^{-ur}}{8\pi u^2}[3/r^3 + 3u/r^2 + u^2/r] + \int_1^\infty \frac{d\zeta}{4\pi}\frac{e^{u\zeta d}-1}{e^{2u\zeta d}-1}u(1-\zeta^2)J_2(ur\sqrt{\zeta^2-1}), \tag{22}$$

$$G_{00}(\mathbf{r};iu) = \frac{e^{-ur}}{-4\pi u^2}[1/r^3 + u/r^2 + u^2/r] + \int_1^\infty \frac{d\zeta}{2\pi}\frac{e^{u\zeta d}+1}{e^{2u\zeta d}-1}u(\zeta^2-1)J_0(ur\sqrt{\zeta^2-1}), \tag{23}$$

where the dependence of $\mathbb{G}$ on $d/2$ has been omitted in its argument for brevity. In all the expressions above the first terms are the components of the Green function in free space, whereas the second terms result from multiple scattering of the cavity plates. As a consequence, the factor $\mathbb{G}^2$ in the integrand of Eq. (20) contains terms with two free-space factors which decay exponentially from $u \approx 2/r$, terms with two multiple-scattering factors which are exponentially suppressed from $u \approx 2/d$, and terms which combine free-space and scattering factors that decay exponentially from $u \approx \min(1/r, 1/d)$.

The calculation of $\langle W_{A,B}/2\rangle_{\rm off}$ requires the numerical integration of Eq. (20), which depends generally on the transition frequencies of both atoms. Nonetheless, assuming that those frequencies are of the same order, say $K \simeq k_{ia}, k_{jb}\ \forall\, i,j$, the dependence of $\langle W_{A,B}/2\rangle_{\rm off}$ on the particular values of transition frequencies and dipole moments can be factored out such that approximately universal potentials can be defined as functions of r and d only. This is, for instance, the case of the vdW interaction between circular Rydberg atoms (see Sec. V below). That is, we can write

$$\langle W_{A,B}/2\rangle_{\rm off} \simeq \frac{-2K^5}{\pi\hbar\epsilon_0^2 c}\sum_{i,j}\mathcal{C}_{ij}\big[\big|d_{i0}^0 d_{0j}^0\big|^2 V_{\rm off}^{00}(r,d) + (|d_{ia}^+ d_{bj}^+|^2 + |d_{ia}^- d_{bj}^-|^2)V_{\rm off}^{++}(r,d) + (|d_{ia}^+ d_{bj}^-|^2 + |d_{ia}^- d_{bj}^+|^2)V_{\rm off}^{+-}(r,d)\big], \tag{24}$$

where $\mathcal{C}_{ij}$ is a numerical factor of order unity whose sign is given by $\mathrm{sgn}(\omega_{ai}\omega_{jb})$; $d_{ia}^p = \langle A_a|d_A^p|A_i\rangle$ is the pth-vector component of the ith transition dipole moment of atom A, and likewise for atom B; and

$$V_{\rm off}^{ps}(r,d) = \int_0^\infty d\chi\ \chi^4 G_{ps}^2(\mathbf{r};iK\chi)/[K(\chi^2+1)]^2, \tag{25}$$

with $p,s = \{+,-,0\}$, are the components in the spherical basis of the dimensionless off-resonant vdW tensor potential, which depend only on r,d. The dimensionless variable of integration χ is the imaginary frequency u in units of K.

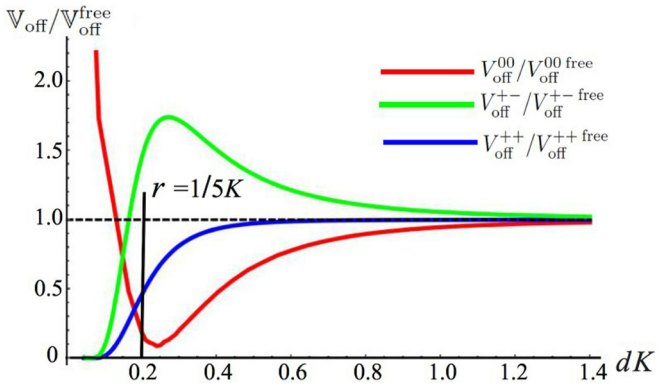

FIG. 4. Graphic representation of the three components of the dimensionless tensor potential $\mathbb{V}_{\rm off}$ of Eq. (25) normalized by their values in free space, $\mathbb{V}_{\rm off}^{\rm free}$. The interatomic distance is fixed at $r = 1/5K$, whereas d varies between 0 and $1.4/K$.

The components of $\mathbb{V}_{\rm off}$ are represented in Fig. 4 as functions of d for a fixed value of the interatomic distance, $r = 1/5K$, normalized by their values in free space. We observe that the effects of the cavity confinement become relevant as d approaches r. Interestingly, three different behaviors are found. Whereas $V_{\rm off}^{++}$ decreases monotonically to zero for $d \ll r$, the component $V_{\rm off}^{+-}$ shows a bump around $d \approx r$, after which it goes to zero as well. In contrast, $V_{\rm off}^{00}$ gets minimum around $d \approx r$ and increases monotonically as d approaches 0. The vanishing of the components $V_{\rm off}^{+-}$ and $V_{\rm off}^{++}$ is an effect of the confinement of the lines of the electric field parallel to the plates. The decrease of both components is indeed exponential as $d/r \to 0$ and so is the decrease of their associated Green's functions, see Eqs. (A3) and (A4). On the contrary, for $d/r \to 0$, the field lines perpendicular to the plates bounce infinite times off the plates when going from one atom to the other, augmenting the strength of $V_{\rm off}^{00}$ as $\sim 1/d^2$. As a matter of fact, G_{00} goes like $1/d$ as $d/r \to 0$, see Eq. (A2).

B. Resonant van der Waals potentials and resonant phase-shift rate

In contrast to the off-resonant interaction, part of the vdW interaction between excited atoms is mediated by virtual photons which resonate with the transitions of one or the other atom, which is referred to as *resonant interaction* [23]. Correspondingly, we refer to the resonant contributions to the potentials and to the phase shift as resonant vdW potentials (res) and resonant phase-shift rate, respectively. On the other hand, these resonant photons mediate also the periodic transfer of the excitation between both atoms. In the perturbative nondegenerate regime this transfer has a small probability proportional to $|\langle W\rangle|/\hbar|\Delta_{AB}| \ll 1$, where Δ_{AB} is the detuning between the relevant transition frequencies of the atoms. It is due to this partial and periodic transfer, as well as to the finite lifetime of excited states, that the vdW potentials with excited atoms become dynamical and are to be computed within the framework of time-dependent perturbation theory [27–30,38,39]. Further, for the usual case that the excitation of the atoms be adiabatic with respect to the detuning Δ_{AB} [27,38], the calculation simplifies to assuming that in the far past the atoms are initially excited and the interaction potential W is turned on adiabatically.

1. Two dissimilar atoms, one of them excited

For the case that the atoms are of different kinds and only one of the them is excited, say atom A at state $a > 0$, while atom B is in its ground state with $b = 0$, only the diagrams (1) and (3) of Figs. 2 and 3 contribute to the resonant potentials of atoms A and B, respectively, yielding [38,39]

$$\langle W_A/2\rangle_{\rm res} = \sum_{j,i<a} \frac{2\omega_{j0}k_{ai}^4}{\epsilon_0^2\hbar\left(\omega_{ai}^2-\omega_{j0}^2\right)} d_{ai}^m d_{0j}^n d_{j0}^p d_{ia}^s \times \{{\rm Re}[G_{mn}(\mathbf{r},k_{ai})]{\rm Re}[G_{ps}(\mathbf{r},k_{ai})] - {\rm Im}[G_{mn}(\mathbf{r},k_{ai})]{\rm Im}[G_{ps}(\mathbf{r},k_{ai})]\}, \quad (26)$$

$$\langle W_B/2\rangle_{\rm res} = \sum_{j,i<a} \frac{2\omega_{j0}k_{ai}^4}{\epsilon_0^2\hbar\left(\omega_{ai}^2-\omega_{j0}^2\right)} d_{ai}^m d_{0j}^n d_{j0}^p d_{ia}^s \times \{{\rm Re}[G_{mn}(\mathbf{r},k_{ai})]{\rm Re}[G_{ps}(\mathbf{r},k_{ai})] + {\rm Im}[G_{mn}(\mathbf{r},k_{ai})]{\rm Im}[G_{ps}(\mathbf{r},k_{ai})]\}, \quad (27)$$

where the tensor indices are $m,n,p,s = \{+,-,0\}$ in the spherical basis and summation over repeated tensor indices is implicit.

For the sake of illustration, we write in Appendix B the explicit expressions of the contributions of diagrams Fig. 2(3) and Fig. 3(2) to $\langle W_A/2\rangle_{\rm res}$ and $\langle W_B/2\rangle_{\rm res}$, respectively. Again, assuming that those frequencies are roughly of the same order, say $K \simeq k_{ai}, k_{j0}\ \forall\, i,j$, Eqs. (26) and (27) can be approximated by

$$\langle W_{A,B}/2\rangle_{\rm res} \simeq \frac{2K^5}{\pi\hbar\epsilon_0^2 c}\sum_{i,j}\mathcal{C}'_{ij}\big[|d_{ia}^0 d_{0j}^0|^2 V_{A,B{\rm res}}^{00}(r,d) + (|d_{ia}^+ d_{0j}^+|^2 + |d_{ia}^- d_{0j}^-|^2)V_{A,B{\rm res}}^{++}(r,d) + (|d_{ia}^+ d_{0j}^-|^2 + |d_{ia}^- d_{0j}^+|^2)V_{A,B{\rm res}}^{+-}(r,d)\big], \quad (28)$$

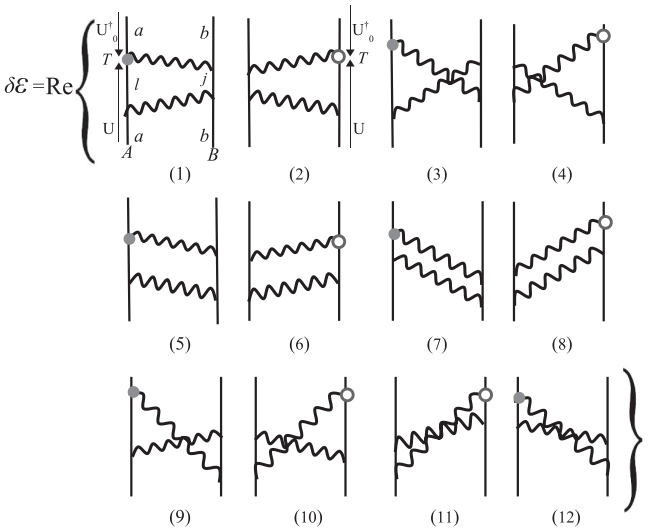

FIG. 5. Diagrammatic representation of the 12 terms which contribute to the phase-shift rate of the two-atom wave function, $\delta\mathcal{E}$. The explanation of the symbols is as in Figs. 2 and 3. Diagrams (1, 3, 5, 7, 9, 12) contain gray circles on the left which stand for the insertion of a Schrödinger operator W_A, whereas diagrams (2, 4, 6, 8, 10, 11) contain white circles on the right which stand for the insertion of an operator W_B. Differently to the diagrams which contribute to $\langle W_A(T)\rangle$ and $\langle W_B(T)\rangle$ in Figs. 2 and 3, respectively, as in diagrams (1) and (2), here the operators W_A or W_B are sandwiched between two time propagators, one of which is the free time-evolution operator, $\mathrm{U}_0(T)$. The explanation of this can be found in Ref. [38].

where $\mathcal{C}'_{ij}$ is a numerical factor of order unity, of the same sign as $\omega_{ai}-\omega_{j0}$, and the dimensionless potentials read

$$V_{A{\rm res}}^{pq}(r,d) = \{{\rm Re}^2[G_{ps}(\mathbf{r},K)] - {\rm Im}^2[G_{ps}(\mathbf{r},K)]\}/K^2, \quad (29)$$

$$V_{B{\rm res}}^{pq}(r,d) = \{{\rm Re}^2[G_{ps}(\mathbf{r},K)] + {\rm Im}^2[G_{ps}(\mathbf{r},K)]\}/K^2, \quad (30)$$

with $p,s = \{+,-,0\}$. As for the resonant phase-shift rate, the addition of diagrams (1) and (3) of Fig. 5 is in this case $\delta\mathcal{E}_{\rm res} = \langle W_A/2\rangle_{\rm res}$ [27,38]. As in free space, it is the discrepancy between the signs of the second terms on the *right-hand side* of Eqs. (29) and (30) that gives rise to a net force on the two-atom system [29,38,39]. The difference is, however, negligible in the nonretarded regime, $rK \lesssim 1$. On the contrary, in the retarded regime, it was already found in Refs. [29,38] that, in free space, while the components of $\mathbb{V}_{A{\rm res}}$ oscillate in space changing sign periodically, the components of $\mathbb{V}_{B{\rm res}}$ decrease monotonically as r increases.

In the presence of a cavity the behavior of the potentials depend on the value of d as well. The components of $\mathbb{V}_{A{\rm res}}$ and $\mathbb{V}_{B{\rm res}}$ are represented in Fig. 6 as functions of the interatomic distance r, with $rK > 1$, for two different values of d, $2/K$ (upper inset) and $20/K$ (lower inset). In contrast to the results in free space, for $d < \pi/K$, only the component $V_{A{\rm res}}^{00}$ oscillates in space, whereas $V_{A{\rm res}}^{++}$ and $V_{A{\rm res}}^{+-}$ decrease monotonically and are equivalent to the potential components of atom B. The reason is that, for $d < \pi/K$,

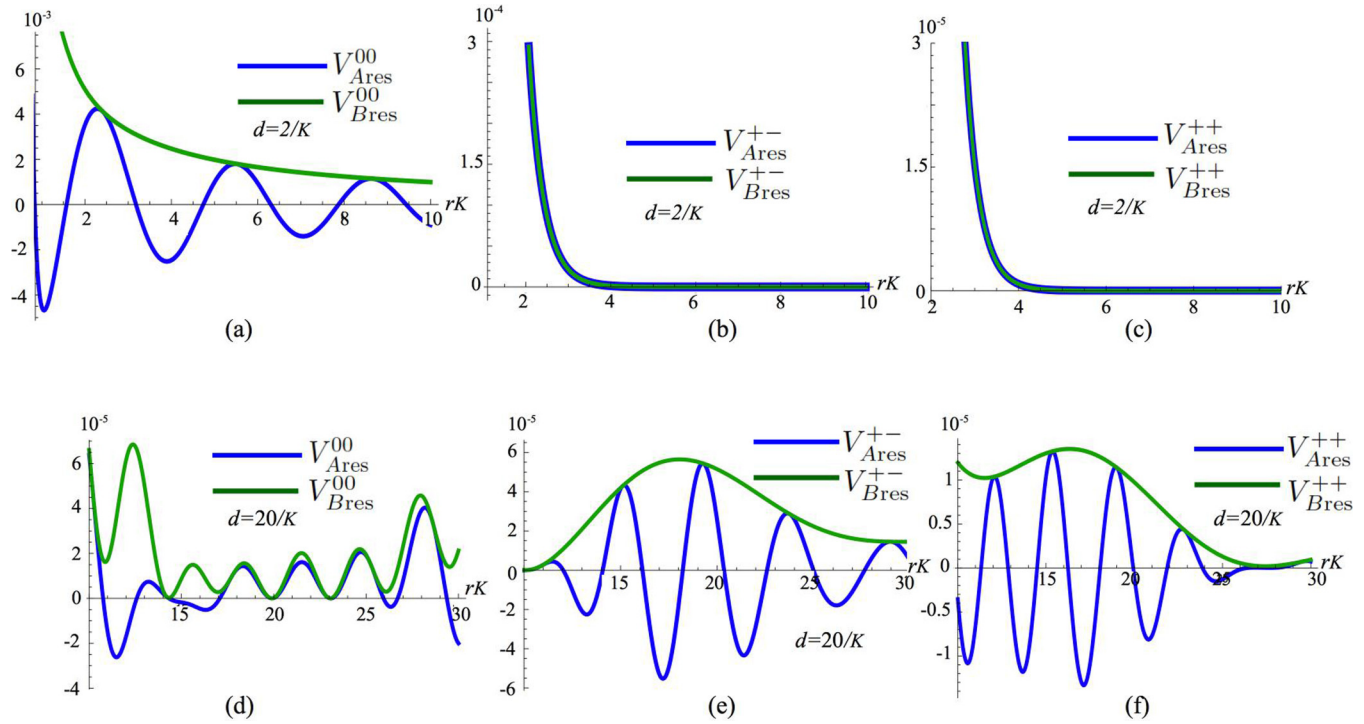

FIG. 6. Graphic representation of the three components of the dimensionless potentials in Eqs. (29) and (30), as functions of rK, for two different values of d, $2/K$ (upper inset) and $20/K$ (lower inset).

only the oscillating terms of G_{00} entering Eqs. (29) and (30) are different from zero, $(1/4d)[Y_0(kr) - i\,J_0(kr)]$. On the contrary, for $d > \pi/K$ (lower inset of Fig. 6) all the components of $\mathbb{V}_{Ares}$ oscillate along r and so do, although with longer periods, the components of $\mathbb{V}_{Bres}$. The latter, however, do not change sign and constitute a sort of envelope of the oscillating curves of $\mathbb{V}_{Ares}$.

2. *Two dissimilar atoms excited*

When both atoms are excited, say on states $a > 0$ and $b > 0$, in addition to diagrams (1) and (3), also the diagrams (2), (4), and (5)–(10) of Figs. 2, 3, and 5 are relevant. The perturbative nondegenerate regime implies in this case that $|\langle W\rangle| \ll \hbar|\omega_{ai} - \omega_{jb}|$, for any pair of intermediate states i, j, with $i < a, j > b$, and $|\langle W\rangle| \ll \hbar|\omega_{bj} - \omega_{ai}|$ for any $i > a, j < b$. For the sake of illustration, explicit expressions of the contributions of diagrams (9) and (10) of Figs. 2, 3, and 5 to $\langle W_A/2\rangle_{\rm res}$, $\langle W_B/2\rangle_{\rm res}$, and $\delta\mathcal{E}_{\rm res}$, respectively, have been included in Appendix B for the case of two dissimilar atoms excited.

Generically, we can distinguish three different contributions to $\langle W_{A,B}/2\rangle_{\rm res}$. These are, a first one in which the intermediate states satisfy $i > a, j < b$, a second one in which they satisfy $i < a, j > b$, and a third one for which $i < a, j < b$. Putting them all together we have

$$
\begin{aligned}
\langle W_A/2\rangle_{\rm res} = &\sum_{j>b,i<a} \frac{2\omega_{jb}k_{ai}^4}{\epsilon_0^2\hbar\left(\omega_{ai}^2-\omega_{jb}^2\right)} d_{ai}^m d_{bj}^n d_{jb}^p d_{ia}^s \{\mathrm{Re}[G_{mn}(\mathbf{r},k_{ai})]\mathrm{Re}[G_{ps}(\mathbf{r},k_{ai})] - \mathrm{Im}[G_{mn}(\mathbf{r},k_{ai})]\mathrm{Im}[G_{ps}(\mathbf{r},k_{ai})]\} \\
&+ \sum_{j<b,i>a} \frac{2\omega_{ia}k_{bj}^4}{\epsilon_0^2\hbar\left(\omega_{bj}^2-\omega_{ia}^2\right)} d_{bj}^m d_{ai}^n d_{ia}^p d_{jb}^s \{\mathrm{Re}[G_{mn}(\mathbf{r},k_{bj})]\mathrm{Re}[G_{ps}(\mathbf{r},k_{bj})] + \mathrm{Im}[G_{mn}(\mathbf{r},k_{bj})]\mathrm{Im}[G_{ps}(\mathbf{r},k_{bj})]\} \\
&- \sum_{j<b,i<a} \frac{2\omega_{bj}k_{ai}^4}{\epsilon_0^2\hbar\left(\omega_{ai}^2-\omega_{bj}^2\right)} d_{ai}^m d_{jb}^n d_{bj}^p d_{ia}^s \{\mathrm{Re}[G_{mn}(\mathbf{r},k_{ai})]\mathrm{Re}[G_{ps}(\mathbf{r},k_{ai})] - \mathrm{Im}[G_{mn}(\mathbf{r},k_{ai})]\mathrm{Im}[G_{ps}(\mathbf{r},k_{ai})]\} \\
&+ \sum_{j<b,i<a} \frac{2\omega_{ai}k_{bj}^4}{\epsilon_0^2\hbar\left(\omega_{ai}^2-\omega_{bj}^2\right)} d_{bj}^m d_{ai}^n d_{ia}^p d_{jb}^s \{\mathrm{Re}[G_{mn}(\mathbf{r},k_{bj})]\mathrm{Re}[G_{ps}(\mathbf{r},k_{bj})] + \mathrm{Im}[G_{mn}(\mathbf{r},k_{bj})]\mathrm{Im}[G_{ps}(\mathbf{r},k_{bj})]\}, \qquad (31) \\
\langle W_B/2\rangle_{\rm res} = &\sum_{j>b,i<a} \frac{2\omega_{jb}k_{ai}^4}{\epsilon_0^2\hbar\left(\omega_{ai}^2-\omega_{jb}^2\right)} d_{ai}^m d_{bj}^n d_{jb}^p d_{ia}^s \{\mathrm{Re}[G_{mn}(\mathbf{r},k_{ai})]\mathrm{Re}[G_{ps}(\mathbf{r},k_{ai})] + \mathrm{Im}[G_{mn}(\mathbf{r},k_{ai})]\mathrm{Im}[G_{ps}(\mathbf{r},k_{ai})]\} \\
&+ \sum_{j<b,i>a} \frac{2\omega_{ia}k_{bj}^4}{\epsilon_0^2\hbar\left(\omega_{bj}^2-\omega_{ia}^2\right)} d_{bj}^m d_{ai}^n d_{ia}^p d_{jb}^s \{\mathrm{Re}[G_{mn}(\mathbf{r},k_{bj})]\mathrm{Re}[G_{ps}(\mathbf{r},k_{bj})] - \mathrm{Im}[G_{mn}(\mathbf{r},k_{bj})]\mathrm{Im}[G_{ps}(\mathbf{r},k_{bj})]\}
\end{aligned}
$$

$$- \sum_{j<b,i<a} \frac{2\omega_{bj}k_{ai}^4}{\epsilon_0^2\hbar\left(\omega_{ai}^2-\omega_{bj}^2\right)} d_{ai}^m d_{jb}^n d_{bj}^p d_{ia}^s \{\mathrm{Re}[G_{mn}(\mathbf{r},k_{ai})]\mathrm{Re}[G_{ps}(\mathbf{r},k_{ai})] + \mathrm{Im}[G_{mn}(\mathbf{r},k_{ai})]\mathrm{Im}[G_{ps}(\mathbf{r},k_{ai})]\}$$

$$+ \sum_{j<b,i<a} \frac{2\omega_{ai}k_{bj}^4}{\epsilon_0^2\hbar\left(\omega_{ai}^2-\omega_{bj}^2\right)} d_{bj}^m d_{ai}^n d_{ia}^p d_{jb}^s \{\mathrm{Re}[G_{mn}(\mathbf{r},k_{bj})]\mathrm{Re}[G_{ps}(\mathbf{r},k_{bj})] - \mathrm{Im}[G_{mn}(\mathbf{r},k_{bj})]\mathrm{Im}[G_{ps}(\mathbf{r},k_{bj})]\}, \quad (32)$$

where the tensor indices are $m,n,p,s = \{+,-,0\}$ in the spherical basis and summation over repeated tensor indices is implicit. Note that analogous expressions were obtained by Barcellona *et al.* in Ref. [29] in free space.

Lastly, as for the phase-shift rate of the two-atom wave function we find,

$$\delta\mathcal{E}_{\mathrm{res}} = \sum_{j>b,i<a} \frac{2\omega_{jb}k_{ai}^4}{\epsilon_0^2\hbar\left(\omega_{ai}^2-\omega_{jb}^2\right)} d_{ai}^m d_{bj}^n d_{jb}^p d_{ia}^s \{\mathrm{Re}[G_{mn}(\mathbf{r},k_{ai})]\mathrm{Re}[G_{ps}(\mathbf{r},k_{ai})] - \mathrm{Im}[G_{mn}(\mathbf{r},k_{ai})]\mathrm{Im}[G_{ps}(\mathbf{r},k_{ai})]\}$$

$$+ \sum_{j<b,i>a} \frac{2\omega_{ia}k_{bj}^4}{\epsilon_0^2\hbar\left(\omega_{bj}^2-\omega_{ia}^2\right)} d_{bj}^m d_{ai}^n d_{ia}^p d_{jb}^s \{\mathrm{Re}[G_{mn}(\mathbf{r},k_{bj})]\mathrm{Re}[G_{ps}(\mathbf{r},k_{bj})] - \mathrm{Im}[G_{mn}(\mathbf{r},k_{bj})]\mathrm{Im}[G_{ps}(\mathbf{r},k_{bj})]\}$$

$$- \sum_{j<b,i<a} \frac{2\omega_{bj}k_{ai}^4}{\epsilon_0^2\hbar\left(\omega_{ai}^2-\omega_{bj}^2\right)} d_{ai}^m d_{jb}^n d_{bj}^p d_{ia}^s \{\mathrm{Re}[G_{mn}(\mathbf{r},k_{ai})]\mathrm{Re}[G_{ps}(\mathbf{r},k_{ai})] - \mathrm{Im}[G_{mn}(\mathbf{r},k_{ai})]\mathrm{Im}[G_{ps}(\mathbf{r},k_{ai})]\}$$

$$+ \sum_{j<b,i<a} \frac{2\omega_{ai}k_{bj}^4}{\epsilon_0^2\hbar\left(\omega_{ai}^2-\omega_{bj}^2\right)} d_{bj}^m d_{ai}^n d_{ia}^p d_{jb}^s \{\mathrm{Re}[G_{mn}(\mathbf{r},k_{bj})]\mathrm{Re}[G_{ps}(\mathbf{r},k_{bj})] - \mathrm{Im}[G_{mn}(\mathbf{r},k_{bj})]\mathrm{Im}[G_{ps}(\mathbf{r},k_{bj})]\}. \quad (33)$$

3. Two identical atoms excited

We consider next the case in which the two atoms are identical, $A = B$, and find in the same excited state $a > 0$. The nondegenerate condition necessary for the calculation to be perturbative and nondegenerate reads in this case $|\langle W\rangle| \ll \hbar|\omega_{ai} - \omega_{ja}|$, for any pair of intermediate states i,j, with $i < a, j > a$.

In comparison to the case of dissimilar atoms, the only difference in the calculation is the presence of double poles when $i = j$ in the frequency integrals which derive from the diagrams (3), (4), (9), and (10). Explicit expressions of the contributions of diagram (4) in Figs. 2 and 5 to $\langle W_A/2\rangle_{\mathrm{res}}$ and $\delta\mathcal{E}_{\mathrm{res}}$, respectively, have been included in Appendix B for this case. As for the resonant vdW potential, it reads,

$$\langle W_A/2\rangle_{\mathrm{res}} = \sum_{i<a,j\neq i} \frac{4\omega_{ja}k_{ai}^4}{\epsilon_0^2\hbar\left(\omega_{ai}^2-\omega_{ja}^2\right)} d_{ai}^m d_{ja}^n d_{aj}^p d_{ia}^s \mathrm{Re}[G_{mn}(\mathbf{r},k_{ai})]\mathrm{Re}[G_{ps}(\mathbf{r},k_{ai})] + \sum_{i<a,j=i} \frac{k_{ai}^2}{\epsilon_0^2 c\hbar} d_{ai}^m d_{ia}^n d_{ai}^p d_{ia}^s$$

$$\times \left\{ k_{ai}\mathrm{Re}[G_{mn}(\mathbf{r},k_{ai})]\mathrm{Re}[G_{ps}(\mathbf{r},k_{ai})] - 2\mathrm{Re}[G_{mn}(\mathbf{r},k_{ai})]\frac{\partial}{\partial k}[k^2\mathrm{Re}[G_{ps}(\mathbf{r},k)]]_{k=k_{ai}} \right\}, \quad (34)$$

whereas the phase-shift rate of the two-atom wave function is

$$\delta\mathcal{E}_{\mathrm{res}} = \sum_{i<a,j\neq i} \frac{4\omega_{ja}k_{ai}^4}{\epsilon_0^2\hbar\left(\omega_{ai}^2-\omega_{ja}^2\right)} d_{ai}^m d_{ja}^n d_{aj}^p d_{ia}^s \{\mathrm{Re}[G_{mn}(\mathbf{r},k_{ai})]\mathrm{Re}[G_{ps}(\mathbf{r},k_{ai})] - \mathrm{Im}[G_{ij}(\mathbf{r},k_{ai})]\mathrm{Im}[G_{ps}(\mathbf{r},k_{ai})]\}$$

$$+ \sum_{i<a,j=i} \frac{k_{ai}^2}{\epsilon_0^2 c\hbar} d_{ai}^m d_{ia}^n d_{ai}^p d_{ia}^s \left\{ k_{ai}\mathrm{Re}[G_{mn}(\mathbf{r},k_{ai})]\mathrm{Re}[G_{ps}(\mathbf{r},k_{ai})] - k_{ai}\mathrm{Im}[G_{mn}(\mathbf{r},k_{ai})]\mathrm{Im}[G_{ps}(\mathbf{r},k_{ai})] \right.$$

$$\left. - 2\mathrm{Re}[G_{mn}(\mathbf{r},k_{ai})]\frac{\partial}{\partial k}[k^2\mathrm{Re}[G_{ps}(\mathbf{r},k)]]_{k=k_{ai}} \right\}. \quad (35)$$

IV. ELECTROSTATIC POTENTIAL BETWEEN INDUCED DIPOLES

Another case of interest commonly encountered in experiments is that of the electrostatic interaction between two atomic dipoles induced by an external static field $\mathbf{E}_0$. The contribution of the 24 diagrams of Fig. 7 reduces to the electrostatic interaction between two induced electric dipoles, A and B, with moments $\alpha_A^a(0)\mathbf{E}_0$ and $\alpha_B^b(0)\mathbf{E}_0$, where $\alpha_{A,B}^{a,b}(0)$ are the static polarizabilities of each atom in the states a and b, respectively. The interaction potentials of each atom coincide in this case, and so does the associated phase-shift rate of the two-atom wave function. If we denote the electrostatic potential by $V_{AB}^{\mathrm{st}}(r)$, it holds $\langle W_A\rangle = \langle W_B\rangle = \delta\mathcal{E}^{\mathrm{st}} \equiv V_{AB}^{\mathrm{st}}(r)$, and

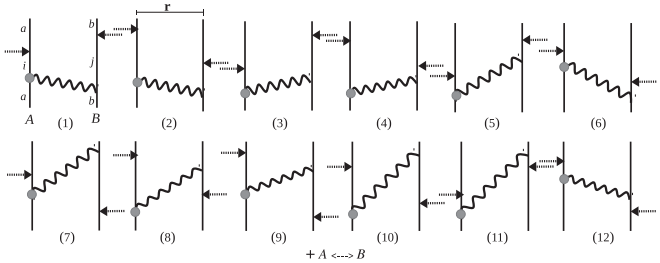

FIG. 7. Diagrammatic representation of the 24 terms (2 times 12 after the exchange $A \leftrightarrow B$) which contribute to $V_{AB}^{\rm st}$ under the action of a constant and uniform external field $\mathbf{E}_0$. Vertices of the interaction Hamiltonian, $-(\mathbf{d}_A + \mathbf{d}_B)\cdot\mathbf{E}_0$, are depicted by horizontal arrows. In diagram (1), the initial states a, b and the generic intermediate states of each atom i, j are indicated. Although not shown, the same states appear in the rest of diagrams in analogous sites.

$\mathbf{F}_{A,B} = \mp\nabla_{\mathbf{r}} V_{AB}^{\rm st}(r)$ for the forces on each atom.[1] The addition of all the contributions of the diagrams of Fig. 7 (which refer to $\langle W_A\rangle$, in particular) yields

$$V_{AB}^{\rm st}(r) = \frac{8}{\pi\epsilon_0 c^2\hbar^2}\sum_{i,j}\frac{\langle a|\mathbf{d}_A|i\rangle\cdot\mathbf{E}_0\langle b|\mathbf{d}_B|j\rangle\cdot\mathbf{E}_0}{\omega_{ia}\omega_{jb}} \times\int_0^\infty d\omega\,\omega{\rm Tr}\{\langle i|\mathbf{d}_A|a\rangle\cdot{\rm Im}[\mathbb{G}(\mathbf{r},d/2;\omega)]\cdot \cdot\langle j|\mathbf{d}_B|b\rangle\}. \tag{36}$$

Next, in application of the Kramers-Kronig relations on the Green function and writing its tensor components in the spherical basis, the above equation can be written as

$$\begin{aligned} V_{AB}^{\rm st}(r) &= \frac{4}{\epsilon_0 c^2\hbar^2}\sum_{i,j}\frac{\langle a|\mathbf{d}_A|i\rangle\cdot\mathbf{E}_0\langle b|\mathbf{d}_B|j\rangle\cdot\mathbf{E}_0}{\omega_{ia}\omega_{jb}}\lim_{\omega\to0}\omega^2 \\ &\quad\times{\rm Tr}\{\langle i|\mathbf{d}_A|a\rangle\cdot{\rm Re}[\mathbb{G}(\mathbf{r},d/2;\omega)]\cdot\langle j|\mathbf{d}_B|b\rangle\} \\ &= \frac{4\pi}{\epsilon_0\hbar^2 d^3}\sum_{i,j}\frac{1}{\omega_{ia}\omega_{jb}}[(|\langle i|d_+^A|a\rangle|^2|\langle j|d_+^B|b\rangle|^2(E_0^+)^2 \\ &\quad+|\langle i|d_-^A|a\rangle|^2|\langle j|d_-^B|b\rangle|^2(E_0^-)^2)V_{++}^{\rm st}(r) \\ &\quad+|\langle i|d_0^A|a\rangle|^2|\langle j|d_0^B|b\rangle|^2\left(E_0^0\right)^2V_{00}^{\rm st}(r) \\ &\quad+(|\langle i|d_+^A|a\rangle|^2|\langle j|d_-^B|b\rangle|^2+|\langle i|d_-^A|a\rangle|^2|\langle j|d_+^B|b\rangle|^2) \\ &\quad\times E_0^-E_0^+V_{+-}^{\rm st}(r)], \end{aligned}$$

where the dimensionless potentials read

$$\begin{aligned} V_{00}^{\rm st}(r) &= 4\sum_{n=1}n^2K_0\left(\frac{2\pi r}{d}n\right), \\ V_{++}^{\rm st}(r) &= \sum_{n=1}\frac{(-1)^n-1}{4}\left[n^2K_0\left(\frac{\pi r}{d}n\right)+\frac{2d}{\pi r}nK_1\left(\frac{\pi r}{d}n\right)\right], \\ V_{+-}^{\rm st}(r) &= \sum_{n=1}\frac{(-1)^n-1}{4}n^2K_0\left(\frac{\pi r}{d}n\right), \end{aligned} \tag{37}$$

[1]Note the absence of the factor 1/2 in the expression for the electrostatic potential in comparison to the vdW potentials. This is due to the fact that the calculation is order 1 in $W_{A,B}$ for $V_{AB}^{\rm st}$ while it is order 2 for the vdW potentials.

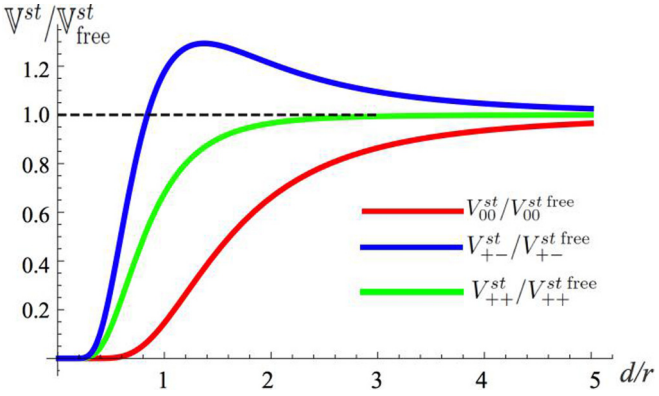

FIG. 8. Graphic representation of the three dimensionless potentials, $V_{00}^{\rm st}$ –red (middle gray) line, $V_{+-}^{\rm st}$ –blue (dark gray) line, and $V_{++}^{\rm st}$ –green (light gray) line, as functions of d/r and normalized by the corresponding potentials in the 3D free space, $V_{00,+-,++}^{st\ \rm free}$.

with K_0 and K_1 being the modified Bessel functions of the second kind, of zero order, and of first order, respectively. In the asymptotic limit $r/d\to0$ the above functions respectively approach the free-space potentials in 3D:

$$\begin{aligned} V_{00}^{\rm st}(r) &\simeq \frac{d^3}{4\pi^2r^3}-\frac{3\,\zeta_R(3)}{4\pi^2}+\frac{3\,\zeta_R(5)}{\pi^2}\frac{r^2}{d^2}, \\ V_{++}^{\rm st}(r) &\simeq -\frac{3d^3}{8\pi^2r^3}+\frac{15\,\zeta_R(5)}{64\pi^2}\frac{r^2}{d^2}, \\ V_{+-}^{\rm st}(r) &\simeq -\frac{d^3}{8\pi^2r^3}-\frac{3\zeta_R(3)}{4\pi^2}+\frac{45\,\zeta_R(5)}{16\pi^2}\frac{r^2}{d^2}, \quad r/d\to0, \end{aligned} \tag{38}$$

where the first terms on the *right-hand side* of each equation are the free-space potentials in 3D and ζ_R is the Riemann ζ function.

In this opposite limit, $d/r\to0$, the functions approach zero exponentially as the EM field is confined to live in 2D:

$$\begin{aligned} V_{00}^{\rm st}(r) &\simeq 2\,e^{-2\pi r/d}\sqrt{d/r}, \\ V_{++}^{\rm st}(r) &\simeq -\frac{1}{2\sqrt{2}}e^{-\pi r/d}\sqrt{d/r}, \\ V_{+-}^{\rm st}(r) &\simeq -\frac{1}{2\sqrt{2}}e^{-\pi r/d}\sqrt{d/r}, \quad d/r\to0. \end{aligned} \tag{39}$$

In Fig. 8, the ratios between the three components of the cavity electrostatic potential and their corresponding values in free space are represented as functions of d/r. While the components $V_{00}^{\rm st}$ and $V_{++}^{\rm st}$ decrease monotonically as d/r decreases, the component $V_{+-}^{\rm st}$ presents a maximum at around $r\approx d$ which overtakes the value in free space.

V. DIPOLE-DIPOLE INTERACTIONS BETWEEN TWO CIRCULAR RYDBERG ATOMS WITHIN A CAVITY

In this section we illustrate the effect of a perfectly reflecting cavity on the dipole-dipole interactions between two identical alkali atoms in Rydberg states. This calculation is of particular relevance to the manipulation of entangled two-atom states [33,34]. A similar calculation has been carried out in Ref. [42] in free space, in the nonretarded regime, and neglecting the off-resonant component of the vdW potential. In our case, in order

to simplify the calculation, we will consider that the atoms are prepared in a certain circular state $|n_c\rangle$. This will allow us to restrict considerably the number of atomic transitions involved in the computations [12,43]. We will consider a pair of alkali atoms, e.g. ^{87}Rb atoms, placed at the middle of a planar cavity and excited at circular Rydberg states. For the calculations in the nondegenerate regime we will take both atoms with $n_c = 50$. At the end of this section and for the sake of completeness, we will compute the Rabi frequency, in the degenerate regime, between two alkali atoms in the states $n_c = 50$ and $n_c' = 51$.

Circular states are the states of maximum angular momentum with quantum numbers $n = n_c$, $l = n_c - 1$, $m = \pm(n_c - 1)$. In a cavity, their stability against mixing with elliptical states of the same energy is achieved by applying an external uniform field $\mathbf{E}_0$ perpendicular to the cavity plates [12,43]. In practice, E_0 is taken large enough so that the corresponding Stark shift lifts the degeneracy between the circular states and the states with $l = n_c - 2$, preventing their mixing due both to the coupling to stray electric fields parallel to the plates and to the vdW interaction between the dipoles. Typical values of E_0 are of the order of 10–100 V/m [12]. With this *proviso*, we proceed to compute the dipole-dipole interactions between two circular Rydberg atoms of ^{87}Rb with $n_c = 50$ and placed at the middle of a cavity of variable width at a fixed interatomic distance, $r = 50$ μm. This is the distance at which retarded effects are not yet relevant and, at the same time, a realistic design of the cavity makes it possible to achieve the condition $d \approx r$, at which the confinement effect of the cavity on the EM field is notorious. Experimentally, the atoms are excited by the action of two pulses, being the typical Rabi frequency of the excitation process much less than the frequency of the atomic transitions involved in the interatomic interaction (cf. Ref. [34]). In addition, the calculation of the resonant component of the vdW interaction meets the conditions outlined in Sec. III B 3. This way, we can fairly apply our perturbative-adiabatic approach to the calculation of all the dipole-dipole interactions between the atoms. Lastly, the fact that the two atoms are identical and excited at the same state guarantees the equivalence between their potentials. The phase-shift rate of the two-atom system is in general different from the potential energy [38]. However, we will show that in the nonretarded regime this discrepancy is negligible for any value of the cavity width. In the following, we compute the electrostatic potential, the off-resonant vdW potential, the resonant vdW potential, and the resonant phase-shift rate for $r = 50$ μm. As for the values of d, we consider the range between 10 μm and 0.50 mm for the calculation of the potentials, and up to 50 mm for the calculation of the phase-shift rate. Atomic data are taken from Ref. [44]. For the calculation of the relevant transition dipole moments we make use of Ref. [43].

In the electrostatic potential between two dipoles induced by an external field $\mathbf{E}_0$ perpendicular to the cavity plates, only the component V_{00}^{st} is nonzero. Labeling the atomic states with the three quantum numbers $|n,l,m\rangle$, at leading order, the intermediate states which enter the sum of $V_{00}^{\mathrm{st}}(r)$ in Eq. (37) are $|n_c+1,n_c,n_c-1\rangle$ and $|n_c+2,n_c,n_c-1\rangle$. The result is depicted graphically in Fig. 9, leaving E_0 as a free parameter.

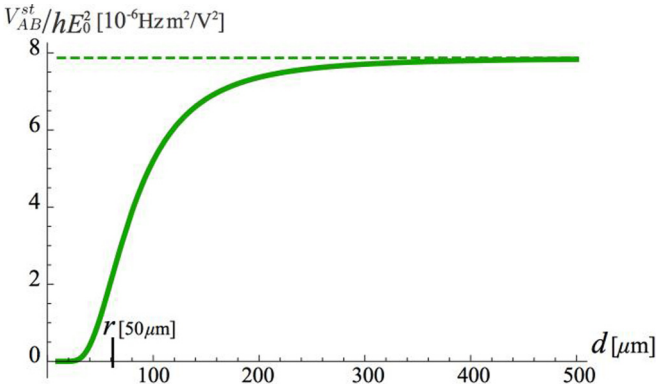

FIG. 9. Graphic representation of the electrostatic potential of two identical Rydberg atoms of ^{87}Rb, in the circular state $n_c = 50$, separated a distance $r = 50$ μm in the middle of a planar cavity of variable width d, subjected to an electric field perpendicular to the cavity plates. The field strength E_0 is left as a free parameter. The dashed line stands for the asymptotic value of the potential in 3D without the cavity.

Regarding the calculation of the off-resonant vdW potential, which is equivalent to the off-resonant phase-shift rate $\delta\mathcal{E}_{\mathrm{off}}$, we first notice that the component V_{off}^{00} in Eq. (24) contains two Π atomic transitions on each atom, whereas the components V_{off}^{++} and V_{off}^{+-} contain pairs of $[\sigma^+]^2$ and $[\sigma^-]^2$ transitions. As explained in Ref. [43], the dipole moments of σ^+ transitions from circular states, $|n_c\rangle$, to the nearest circular states, $|(n \pm 1)_c\rangle$, are of the order of n_c times greater than those of Π transitions and n_c^2 times greater than those of σ^- transitions. Therefore, the off-resonant vdW potential will be dominated by the component V_{off}^{++} and the transition wavelengths $\lambda_{51,50} \approx \lambda_{50,49} \simeq 6$ mm. The result is shown graphically by the red (middle gray) curve of Fig. 10.

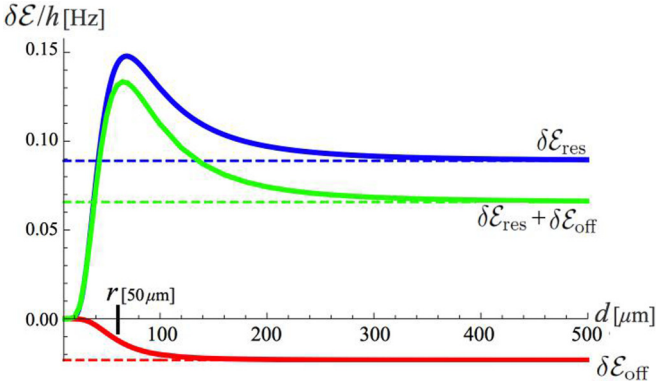

FIG. 10. Graphic representation of the phase-shift rate $\delta\mathcal{E}$ (equivalently, vdW potential) of two identical Rydberg atoms of ^{87}Rb, in the circular state $n_c = 50$, separated a distance $r = 50$ μm in the middle of a planar cavity of variable width d. The off-resonant, resonant, and total phase-shift rates are represented separately by the lines in red (middle gray), blue (dark gray), and green (light gray), respectively. Dashed lines stand for the asymptotic values of the energies in free space.

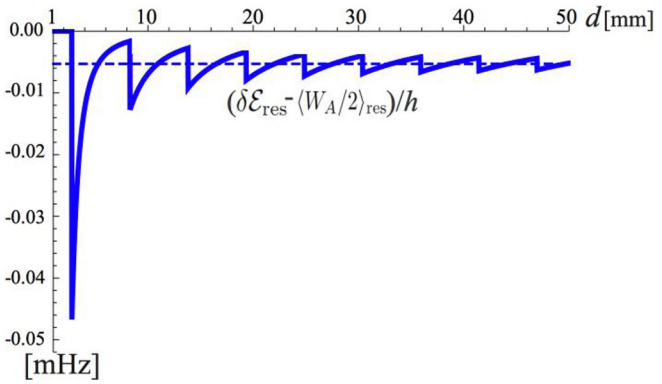

FIG. 11. Graphic representation of the difference between the resonant phase-shift rate, $\delta\mathcal{E}_{res}$, and the resonant vdW potential, $\langle W_A/2\rangle_{\rm res}$, of two identical Rydberg atoms of ^{87}Rb, in the circular state $n_c = 50$, separated a distance $r = 50\ \mu$m in the middle of a planar cavity of variable width d. The dashed line stands for the asymptotic value of the energy difference in free space.

Finally, concerning the calculation of the resonant vdW potential, it is dominated by the dyadic components $+-$ of Eq. (34), in which the leading terms are proportional to the transition dipole moments between the states $|n_c\rangle$ and $|(n \pm 1)_c\rangle$ [43]. In particular, the greatest contribution comes from the quasiresonant diagram (1) of Fig. 3, which includes a term proportional to the inverse of the detuning, $1/(\omega_{50,49} - \omega_{51,50})$ [38]. The resonant vdW potential is depicted graphically by the blue (dark gray) line in Fig. 10. It is worth noting that the resonant phase-shift rate $\delta\mathcal{E}_{\rm res}$ coincides with the resonant vdW potential for $d \lesssim 3$ mm. The reason is that the imaginary part of the Green function which enters Eq. (35) vanishes unless $d \geqslant \lambda_{51,50}/2 \approx 3$ mm. For greater values of d, resonances show up with periodicity $\simeq$6 mm. This is shown in Fig. 11, where the difference between $\delta\mathcal{E}_{\rm res}$ and $\langle W_A/2\rangle_{\rm res}$ is represented. In the nonretarded regime this difference is 7 orders of magnitude less than $\delta\mathcal{E}_{\rm res}$, and is hence negligible.

The graphs represented in Fig. 10 show that for cavity widths much smaller than the interatomic distance the strength of the vdW interaction decreases exponentially, whereas for values of d close to r the strength of the interaction is higher than its value in the absence of cavity. The latter is a consequence of the dominance of the dyadic components $+-$ in the resonant vdW potential. It is also worth mentioning that, even in free space, the ratio between the strength of the off-resonant (red line of Fig. 10) and the strength of the resonant vdW potentials (green line) is approximately 1/5 but not negligible, in contradiction to what is usually assumed in the literature for the binary interactions between Rydberg atoms (see, e.g., Ref. [42]).

We conclude this section with the calculation of the Rabi frequency induced by the cavity field on the symmetric states $|50_c,51_c\rangle$ and $|51_c,50_c\rangle$ of two atoms of ^{87}Rb separated 50 μm. A rigorous time-dependent treatment of this interaction is complicated since the adiabatic approximation considered in our previous calculations is not valid generally [45], the reason being that the interaction takes place in the degenerate regime. However, in the nonretarded regime a great simplification is possible. It suffices to consider the diagrams of the kind of

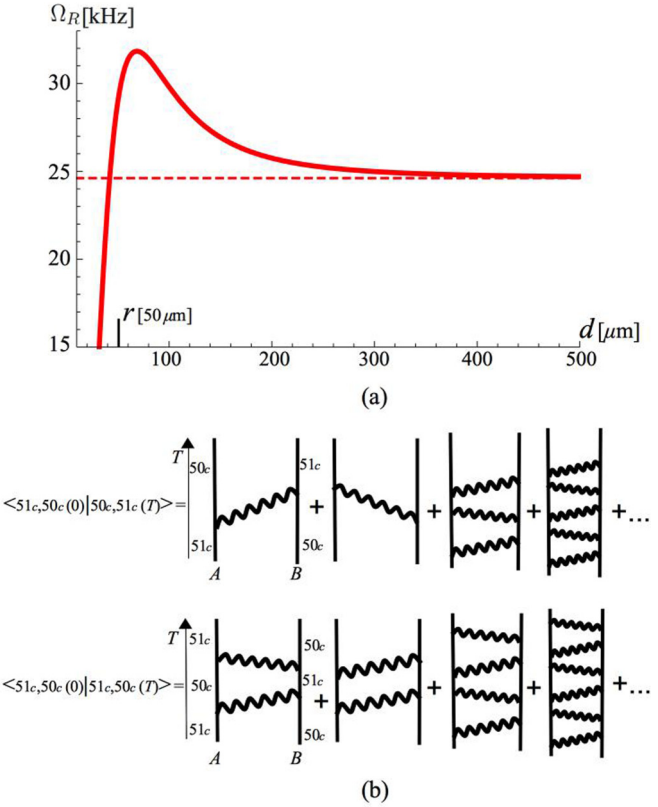

FIG. 12. (a) Graphic representation of the Rabi frequency induced by the cavity field on the symmetric states $|50_c,51_c\rangle$ and $|51_c,50_c\rangle$ of two ^{87}Rb atoms separated a distance $r = 50\ \mu$m in the middle of a planar cavity of variable width d. The dashed line stands for the asymptotic value of the Rabi frequency in 3D without the cavity. (b) Diagrammatic representation of the processes which contribute to the probability amplitudes $\langle 51_c,50_c\,(0)|50_c,51_c\,(T)\rangle$ and $\langle 51_c,50_c\,(0)|51_c,50_c\,(T)\rangle$. In all the diagrams the circular states 50_c and 51_c (only shown in the first diagrams on the *right-hand side* of the equalities) alternate after each vertex of interaction along the temporal vertical axis. Note that whereas in the diagrams contributing to $\langle 51_c,50_c\,(0)|50_c,51_c\,(T)\rangle$ the initial and final states differ, they coincide in those for $\langle 51_c,50_c\,(0)|51_c,50_c\,(T)\rangle$. Hence, while $\langle 51_c,50_c\,(0)|50_c,51_c\,(T)\rangle$ is proportional to $\sin(\Omega_R T/2)$, $\langle 51_c,50_c\,(0)|51_c,50_c\,(T)\rangle$ is proportional to $\cos(\Omega_R T/2)$ instead.

those in Fig. 12(b), in which the circular states 50_c and 51_c alternate after each vertex of interaction and only one-photon states appear as intermediate states. The net result is a Rabi oscillation of frequency Ω_R between the states $|50_c,51_c\rangle$ and $|51_c,50_c\rangle$. As shown in Ref. [46], this approach is equivalent to the usual one based on degenerate stationary perturbation theory in the subspace $\{|50_c,51_c\rangle, |51_c,50_c\rangle\}$ [47]. For this reason, and just for the sake of illustration, we will restrict ourselves to the nonretarded regime in which the expression of the Rabi frequency Ω_R associated reads

$$\Omega_R \simeq \frac{2\pi}{\epsilon_0\hbar d^3}\langle 50_c|\mathbf{d}|51_c\rangle \cdot \mathbb{V}^{\rm st} \cdot \langle 51_c|\mathbf{d}|50_c\rangle, \qquad (40)$$

where the only component of $\mathbb{V}^{\rm st}$ which enters Eq. (40) is $V^{\rm st}_{+-}$. The graph of Fig. 12(a) shows the variation of Ω_R with the cavity width d.

VI. CONCLUSIONS

In this article we have computed the dyadic Green's function of the cavity field which mediates the interaction between two atomic dipoles placed in the middle of a perfectly reflecting planar cavity. The components of the Green tensor are given in Eqs. (9)–(14) and as a series in the number of reflections in Eqs. (15)–(17). Asymptotic expressions in the 2D and 3D limits can be found in Appendix A.

The van der Waals potentials of each atom as well as the associated phase-shift rates of their wave function have been calculated in the weak-coupling, nondegenerate regime for several cases of interest: for the case that both atoms are in their ground states, for the case that both atoms are excited, and for the case that one atom is excited while the other, of a different kind, is in its ground state. The discrepancies between the resonant components of the vdW potentials and the phase-shift rates have been exposed for each case. However, those discrepancies are relevant only in the retarded regime and, generally, for cavity widths larger than half the resonant wavelengths, see Figs. 6 and 11. In addition, we have calculated the electrostatic potential between two induced atomic dipoles [Eqs. (37)–(39)]. The latter has been used also to compute the Rabi frequency on a two-Rydberg-atom state in the degenerate regime [Eq. (40), Fig. 12].

The effect of the two-dimensional confinement of the electromagnetic field by the cavity on the dipole-dipole interactions has been analyzed. The effect depends on the atomic polarization of induced and fluctuating dipoles. For values of the cavity width much less than the interatomic distance, for dipole moments oriented parallel to the plates, both the electrostatic and the vdW interactions are exponentially suppressed; on the contrary, for dipole moments perpendicular to the plates, while the electrostatic interaction decreases exponentially, too, the strength of the off-resonant vdW interaction increases with respect to its value in the absence of cavity (Figs. 4 and 8). These behaviors can be explained by the asymptotic expressions of the Green's function components in the 2D limit [see Eqs. (39), (A2)–(A4)]. For values of the cavity width close to the interatomic separation, $d \approx r$, for dipole moments oriented parallel to the plates, the strengths of both the electrostatic and the vdW interactions are larger than their values in the absence of cavity; on the contrary, for dipole moments perpendicular to the plates, the vdW interaction presents a minimum much less than its value in the absence of cavity.

The confinement effects have been illustrated in Sec. V through the computation of the dipole-dipole interactions between two circular Rydberg atoms of ^{87}Rb. As shown in Fig. 10, for cavity widths much smaller than the interatomic distance, the strength of the vdW interaction decreases exponentially, whereas for values of d close to r the strength of the interaction is larger than its value in the absence of cavity. The inhibition or the enhancement of the vdW interaction may have an impact on the experimental manipulation of entangled atomic states, for instance, in the Rydberg blockade regime [33,34]. In this regime, however, the interatomic distance lies in the range of 1–10 μm, which is much less than any realistic value of the width of a metallic cavity. For $d \lesssim 10\ \mu$m the stray charges on the plates would have a strong influence on the plate-atom interaction, disturbing the experimental measurements. Therefore, other materials should be used in the construction of the cavity to diminish these unwanted effects. Nonetheless, confinement effects in metallic cavities could be still relevant in the retarded regime of the vdW interaction.

The application of our approach to the cavity-assisted interaction between atomic dipoles in the strong coupling regime, of interest in the building of quantum gates with neutral atoms [15,48], is left for future work.

ACKNOWLEDGMENTS

We thank M.-P. Gorza, M. Brune, J.-M. Raimond, A. Lambrecht, and S. Reynaud for useful discussions on this problem. Financial support from French Contracts No. ANR-10-IDEX-0001-02-PSL and No. ANR-13-BS04–0003-02, and from Spanish Grants No. MTM2014-57129-C2-1-P (MINECO) and No. VA057U16 (Junta de Castilla y León and FEDER) are gratefully acknowledged.

APPENDIX A: ASYMPTOTIC EXPRESSIONS OF THE GREEN DYADIC COMPONENTS OF THE CAVITY FIELD

The expressions of the Green dyadic components computed in Sec. II adopt the following form in the 3D limit, $d \gg r, k^{-1}$, in the spherical basis:

$$
\begin{aligned}
G_{00}(\mathbf{r},d/2;k) &\simeq \frac{e^{ikr}}{-4\pi k^2}\left[\frac{-1}{r^3}+\frac{ik}{r^2}+\frac{k^2}{r}\right]+i\,\frac{e^{ikd}}{\pi k\, d^2}(1+i/kd)+\frac{e^{ikd}}{\pi}\frac{r^2}{d^3}(1+3i/kd-3/k^2d^2),\\
G_{++}(\mathbf{r},d/2;k) &\simeq \frac{e^{ikr}}{8\pi k^2}[3/r^3-3ik/r^2-k^2/r]-\frac{e^{ikd}}{4\pi}\frac{r^2}{d^3}(1+3i/kd-1/k^2d^2),\\
G_{+-}(\mathbf{r},d/2;k) &\simeq \frac{e^{ikr}}{8\pi k^2}[1/r^3-ik/r^2+k^2/r]+\frac{1}{\pi d}[\log(1-e^{ikd})+i\,e^{ikd}/kd-e^{ikd}/k^2d^2]\\
&\quad +i\,k\frac{e^{ikd}}{2\pi}\frac{r^2}{d^2}(1+3i/kd-6/k^2d^2-6i/k^3d^3),\quad d\gg r,k^{-1}.
\end{aligned}
\tag{A1}
$$

As for the 2D limit, $d \ll r,k^{-1}$, the dyadic components read

$$G_{00}(\mathbf{r},d/2;k) \simeq \frac{1}{4d}[Y_0(kr) - i\, J_0(kr)] + \frac{2\pi e^{-2\pi r/d}}{k^2 d^2\sqrt{rd}}(1 - k^2d^2/4\pi^2), \tag{A2}$$

$$G_{++}(\mathbf{r},d/2;k) \simeq \frac{-\pi e^{-\pi r/d}}{2\sqrt{2}k^2d^2\sqrt{rd}}(1 + k^2d^2/\pi^2), \tag{A3}$$

$$G_{+-}(\mathbf{r},d/2;k) \simeq \frac{-\pi e^{-\pi r/d}}{2\sqrt{2}k^2d^2\sqrt{rd}}(1 + 2d/\pi r - k^2d^2/\pi^2), \quad d \ll r,k^{-1}. \tag{A4}$$

APPENDIX B: RESONANT CONTRIBUTIONS OF SOME DIAGRAMS TO THE VAN DER WAALS POTENTIALS AND PHASE-SHIFT RATES

In the following, we write the expressions of the resonant contributions of some diagrams to the vdW potentials and phase-shift rates at order four in W. The rules to read off each diagram are as follows. The four vertices yield a tensor factor $\frac{2\alpha_f c^3}{\pi\epsilon_0 e^2} d^m_{ai} d^n_{jb} d^p_{jb} d^s_{ai}$; each wavy line contributes with a cavity field Green's function, $k^2 \mathrm{Im} G_{ps}(\mathbf{r},k)$; and free time-propagators are inserted between any pair of consecutive vertices, with time evolving from above and from below in the far past, towards the observable vertex at instant T, as sketched in diagram (1) of Figs. 2 and 3, and in diagrams (1) and (2) of Fig. 5.

For the case of one atom excited, we give the expressions of the contributions of diagrams Fig. 2(3) and Fig. 3(2) to $\langle W_A/2\rangle_{\mathrm{res}}$ and $\langle W_B/2\rangle_{\mathrm{res}}$, respectively, in the adiabatic approximation. As for diagram Fig. 2(3), its contribution to $\langle W_A/2\rangle_{\mathrm{res}}$ is

$$\begin{aligned}
&\frac{2\alpha_f c^3}{\pi\epsilon_0 e^2} \sum_{i<a,j} d^m_{ai} d^n_{j0} d^p_{j0} d^s_{ai} \int_{-\infty}^{+\infty} dk\, k^2 \mathrm{Im} G_{mn}(\mathbf{r},k) \int_{-\infty}^{+\infty} dk'\, k'^2 \mathrm{Im} G_{ps}(\mathbf{r},k') \\
&\quad \times \int_{-\infty}^{T} dt \int_{-\infty}^{t} dt' \int_{-\infty}^{t'} dt''\, e^{\eta(t+t'+t'')} [(i\, e^{i\omega_{ai}T} e^{-i(T-t)\omega} e^{-i(t-t')(\omega+\omega'+\omega_{j0})} e^{-i(t'-t'')\omega'} e^{-it''\omega_{ai}}) + (\omega \leftrightarrow \omega')^*] \\
&= \frac{-4\alpha_f c^3}{\pi\epsilon_0 e^2} \mathrm{Re} \sum_{i<a,j} d^m_{ai} d^n_{j0} d^p_{j0} d^s_{ai} \int_{-\infty}^{+\infty} dk \int_{-\infty}^{+\infty} \frac{dk'\, k^2 \mathrm{Im} G_{mn}(\mathbf{r},k)\, k'^2 \mathrm{Im} G_{ps}(\mathbf{r},k')}{[\omega + \omega' - (\omega_{ai} - \omega_{j0})](\omega - \omega_{ai} - i\eta)(\omega' - \omega_{ai} - i\eta)}, \ \eta \to 0^+,
\end{aligned} \tag{B1}$$

where a summation over repeated tensor indices is implicit. The contribution of diagram Fig. 3(2) to $\langle W_B/2\rangle_{\mathrm{res}}$ reads

$$\begin{aligned}
&\mathrm{Re}\frac{2\alpha_f c^3}{\pi\epsilon_0 e^2} \sum_{i<a,j} d^m_{ai} d^n_{j0} d^p_{j0} d^s_{ai} \int_{-\infty}^{+\infty} dk\, k^2 \mathrm{Im} G_{mn}(\mathbf{r},k) \int_{-\infty}^{+\infty} dk'\, k'^2 \mathrm{Im} G_{ps}(\mathbf{r},k') \\
&\quad \times \int_{-\infty}^{T} dt \int_{-\infty}^{t} dt' \int_{-\infty}^{T} dt''\, e^{\eta(t+t'+t'')} [(-i e^{i(T-t)\omega_B} e^{i(t-t')\omega} e^{i\omega_A t'}\, e^{-i(T-t'')\omega'} e^{-it''\omega_A}) + (\omega \leftrightarrow \omega')] \\
&= \frac{4\alpha_f c^3}{\pi\epsilon_0 e^2} \mathrm{Re} \sum_{i<a,j} d^m_{ai} d^n_{j0} d^p_{j0} d^s_{ai} \int_{-\infty}^{+\infty} dk \int_{-\infty}^{+\infty} dk' \frac{k^2 \mathrm{Im} G_{mn}(\mathbf{r},k)\, k'^2 \mathrm{Im} G_{ps}(\mathbf{r},k')}{(\omega_{ai} - \omega_{j0})(\omega - \omega_{ai} - i\eta)(\omega' - \omega_{ai} + i\eta)}, \ \eta \to 0^+.
\end{aligned} \tag{B2}$$

As for the case of two dissimilar atoms excited, we give the expressions of the contributions of diagrams (9) and (10) of Figs. 2, 3, and 5 to $\langle W_A/2\rangle_{\mathrm{res}}$, $\langle W_B/2\rangle_{\mathrm{res}}$, and $\delta\mathcal{E}_{\mathrm{res}}$, respectively, in the adiabatic approximation. The contributions of diagram (9) are, respectively,

$$\begin{aligned}
&\frac{2\alpha_f c^3}{\pi\epsilon_0 e^2} \sum_{i<a,j<b} d^m_{ai} d^n_{jb} d^p_{jb} d^s_{ai} \int_{-\infty}^{+\infty} dk\, k^2 \mathrm{Im} G_{mn}(\mathbf{r},k) \int_{-\infty}^{+\infty} dk'\, k'^2 \mathrm{Im} G_{ps}(\mathbf{r},k') \\
&\quad \times \Bigg[\int_{-\infty}^{T} dt \int_{-\infty}^{t} dt' \int_{-\infty}^{t'} dt''\, e^{\eta(t+t'+t'')} (i\, e^{-i(T-t)(\omega+\omega_{bj})} e^{-i(t-t')(\omega+\omega')} e^{-i(t'-t'')(\omega+\omega_{ai})} e^{-it''(\omega_{ai}+\omega_{bj})}) \\
&\quad + \int_{-\infty}^{T} dt \int_{-\infty}^{T} dt' \int_{-\infty}^{t'} dt''\, e^{\eta(t+t'+t'')} i\, e^{i(\omega_{ai}+\omega_{bj})T} e^{-i(T-t)(\omega+\omega_{ai})} e^{-it(\omega_{ai}+\omega_{bj})} e^{i(T-t')(\omega+\omega')} e^{i(t'-t'')(\omega+\omega_{bj})} e^{it''(\omega_{ai}+\omega_{bj})} \Bigg] \\
&= \frac{-2\alpha_f c^3}{\pi\epsilon_0 e^2} \mathrm{Re} \sum_{i<a,j<b} d^m_{ai} d^n_{jb} d^p_{jb} d^s_{ai} \int_{-\infty}^{+\infty} dk \int_{-\infty}^{+\infty} dk' \Bigg[\frac{k^2 \mathrm{Im} G_{mn}(\mathbf{r},k)\, k'^2 \mathrm{Im} G_{ps}(\mathbf{r},k')}{(\omega + \omega' - \omega_{ai} - \omega_{bj} - 2i\eta)(\omega - \omega_{bj} - i\eta)(\omega - \omega_{ai} - 3i\eta)} \\
&\quad + \frac{k^2 \mathrm{Im} G_{mn}(\mathbf{r},k)\, k'^2 \mathrm{Im} G_{ps}(\mathbf{r},k')}{(\omega + \omega' - \omega_{ai} - \omega_{bj} + 2i\eta)(\omega - \omega_{bj} - i\eta)(\omega - \omega_{ai} + i\eta)} \Bigg], \quad \eta \to 0^+, \text{ to } \langle W_A/2\rangle_{\mathrm{res}};
\end{aligned} \tag{B3}$$

$$\frac{2\alpha_f c^3}{\pi\epsilon_0 e^2}\sum_{i<a,j<b} d^m_{ai}d^n_{jb}d^p_{jb}d^s_{ai}\int_{-\infty}^{+\infty}dk\,k^2\mathrm{Im}G_{mn}(\mathbf{r},k)\int_{-\infty}^{+\infty}dk'\,k'^2\mathrm{Im}G_{ps}(\mathbf{r},k')$$
$$\times\left[\int_{-\infty}^{T}dt\int_{-\infty}^{t}dt'\int_{-\infty}^{T}dt''\,e^{\eta(t+t'+t'')}(-i\,e^{-i(T-t)(\omega+\omega')}e^{-i(t-t')(\omega+\omega_{ai})}e^{-it'(\omega_{bj}+\omega_{ai})}e^{i(T-t'')(\omega+\omega_{bj})}e^{it''(\omega_{ai}+\omega_{bj})})\right.$$
$$\left.+\int_{-\infty}^{T}dt\int_{-\infty}^{t}dt'\int_{-\infty}^{t'}dt''\,e^{\eta(t+t'+t'')}(-i\,e^{-i(\omega_{ai}+\omega_{bj})T}e^{i(T-t)(\omega+\omega_{ai})}e^{i(t-t')(\omega+\omega')}e^{i(t'-t'')(\omega+\omega_{bj})}e^{it''(\omega_{ai}+\omega_{bj})})\right]$$
$$=\frac{-2\alpha_f c^3}{\pi\epsilon_0 e^2}\mathrm{Re}\sum_{i<a,j<b} d^m_{ai}d^n_{jb}d^p_{jb}d^s_{ai}\int_{-\infty}^{+\infty}dk\int_{-\infty}^{+\infty}dk'\left[\frac{k^2\mathrm{Im}G_{mn}(\mathbf{r},k)\,k'^2\mathrm{Im}G_{ps}(\mathbf{r},k')}{(\omega+\omega'-\omega_{ai}-\omega_{bj}-2i\eta)(\omega-\omega_{ai}+i\eta)(\omega-\omega_{bj}-i\eta)}\right.$$
$$\left.+\frac{k^2\mathrm{Im}G_{mn}(\mathbf{r},k)\,k'^2\mathrm{Im}G_{ps}(\mathbf{r},k')}{(\omega+\omega'-\omega_{ai}-\omega_{bj}+2i\eta)(\omega-\omega_{ai}+i\eta)(\omega-\omega_{bj}+3i\eta)}\right],\quad \eta\to 0^+,\ \text{to}\ \langle W_B/2\rangle_{\mathrm{res}};\tag{B4}$$

and

$$\frac{2\alpha_f c^3}{\pi\epsilon_0 e^2}\sum_{i<a,j<b} d^m_{ai}d^n_{jb}d^p_{jb}d^s_{ai}\int_{-\infty}^{+\infty}dk\,k^2\mathrm{Im}G_{mn}(\mathbf{r},k)\int_{-\infty}^{+\infty}dk'\,k'^2\mathrm{Im}G_{ps}(\mathbf{r},k')$$
$$\times\int_{-\infty}^{T}dt\int_{-\infty}^{t}dt'\int_{-\infty}^{t'}dt''\,e^{\eta(t+t'+t'')}(i\,e^{-i(T-t)(\omega+\omega_{bj})}e^{-i(t-t')(\omega+\omega')}e^{-i(t'-t'')(\omega+\omega_{ai})}e^{-it''(\omega_{ai}+\omega_{bj})})$$
$$=\frac{-2\alpha_f c^3}{\pi\epsilon_0 e^2}\mathrm{Re}\sum_{i<a,j<b} d^m_{ai}d^n_{jb}d^p_{jb}d^s_{ai}\int_{-\infty}^{+\infty}dk\int_{-\infty}^{+\infty}\frac{dk'\,k^2\mathrm{Im}G_{mn}(\mathbf{r},k)\,k'^2\mathrm{Im}G_{ps}(\mathbf{r},k')}{(\omega+\omega'-\omega_{ai}-\omega_{bj}-2i\eta)(\omega-\omega_{bj}-i\eta)(\omega-\omega_{ai}-3i\eta)},\ \eta\to 0^+,\tag{B5}$$

to $\delta\mathcal{E}_{\mathrm{res}}$.

The corresponding contributions of diagram (10) are identical to those of diagram (9), but for the exchange of subindices $ai\leftrightarrow bj$ in all the expressions above.

Finally, for the case of two identical atoms excited, in the perturbative regime, we give the expressions of the contributions of diagram (4) of Figs. 2 and 5, with double poles, to $\langle W_A/2\rangle_{\mathrm{res}}$ and $\delta\mathcal{E}_{\mathrm{res}}$, respectively, in the adiabatic approximation. These are,

$$\frac{4\alpha_f c^3}{\pi\epsilon_0 e^2}\mathrm{Re}\sum_{i<a} d^m_{ai}d^n_{ai}d^p_{ai}d^s_{ai}\int_{-\infty}^{+\infty}dk\,k^2\mathrm{Im}G_{mn}(\mathbf{r},k)\int_{-\infty}^{+\infty}dk'\,k'^2\mathrm{Im}G_{ps}(\mathbf{r},k')$$
$$\times\int_{-\infty}^{T}dt\int_{-\infty}^{T}dt'\int_{-\infty}^{t'}dt''\,e^{\eta(t+t'+t'')}(-i\,e^{i(T-t)(\omega+\omega_{ai})}e^{2it\omega_{ai}}e^{-i(T-t')(\omega+\omega')}e^{-i(t'-t'')(\omega'+\omega_{ai})}e^{-2it''\omega_{ai}})$$
$$=\frac{-4\alpha_f c^3}{\pi\epsilon_0 e^2}\mathrm{Re}\sum_{i<a} d^m_{ai}d^n_{ai}d^p_{ai}d^s_{ai}\int_{-\infty}^{+\infty}dk\int_{-\infty}^{+\infty}\frac{dk'\,k^2\mathrm{Im}G_{mn}(\mathbf{r},k)\,k'^2\mathrm{Im}G_{ps}(\mathbf{r},k')}{(\omega+\omega'-2\omega_{ai}-2i\eta)(\omega'-\omega_{ai}-i\eta)(\omega-\omega_{ai}+i\eta)},\ \eta\to 0^+,\tag{B6}$$

to $\langle W_A/2\rangle_{\mathrm{res}}$; and

$$\frac{4\alpha_f c^3}{\pi\epsilon_0 e^2}\mathrm{Re}\sum_{i<a} d^m_{ai}d^n_{ai}d^p_{ai}d^s_{ai}\int_{-\infty}^{+\infty}dk\,k^2\mathrm{Im}G_{mn}(\mathbf{r},k)\int_{-\infty}^{+\infty}dk'\,k'^2\mathrm{Im}G_{ps}(\mathbf{r},k')$$
$$\times\int_{-\infty}^{T}dt\int_{-\infty}^{t}dt'\int_{-\infty}^{t'}dt''\,e^{\eta(t+t'+t'')}(i\,e^{2iT\omega_{ai}}e^{i(T-t)(\omega+\omega_{ai})}e^{-i(t-t')(\omega+\omega')}e^{-i(t'-t'')(\omega'+\omega_{ai})}e^{-2it''\omega_{ai}})$$
$$=\frac{-4\alpha_f c^3}{\pi\epsilon_0 e^2}\mathrm{Re}\sum_{i<a} d^m_{ai}d^n_{ai}d^p_{ai}d^s_{ai}\int_{-\infty}^{+\infty}dk\int_{-\infty}^{+\infty}\frac{dk'\,k^2\mathrm{Im}G_{mn}(\mathbf{r},k)\,k'^2\mathrm{Im}G_{ps}(\mathbf{r},k')}{(\omega+\omega'-2\omega_{ai}-2i\eta)(\omega'-\omega_{ai}-i\eta)(\omega-\omega_{ai}-3i\eta)},\ \eta\to 0^+,\tag{B7}$$

to $\delta\mathcal{E}_{\mathrm{res}}$. In this case, the results of the frequency integrals in Eqs. (B6) and (B7) coincide.

[1] P. R. Berman, *Cavity Quantum Electrodynamics* (Academic Press, New York, 1994).

[2] H. Walther, B. T. H. Varcoe, B. G. Englert, and T. Becke, Rep. Prog. Phys. **69**, 1325 (2006).

[3] Y. Kaluzny, P. Goy, M. Gross, J. M. Raimond, and S. Haroche, Phys. Rev. Lett. **51**, 1175 (1983).

[4] G. Barton, Proc. Roy. Soc. Lond. A **367**, 117 (1979); **410**, 141 (1987).

[5] A. A. Belov, Yu. E. Lozovik, and V. L. Pokrovskii, Sov. Phys. JETP **69**, 312 (1989).

[6] E. A. Hinds and V. Sandoghdar, Phys. Rev. A **43**, 398 (1991).

[7] W. Jhe, Phys. Rev. A **43**, 5795 (1991); **44**, 5932 (1991).

[8] C. A. Lütken and F. Ravndal, Phys. Rev. A **31**, 2082 (1985).

[9] P. W. Milonni, *The Quantum Vacuum* (Academic Press, San Diego, CA, 1994).

[10] P. W. Milonni and P. L. Knight, Opt. Commun. **9**, 119 (1973).

[11] H. Nha and W. Jhe, Phys. Rev. A **54**, 3505 (1996).

[12] P. Nussenzveig, F. Bernardot, M. Brune, J. Hare, J. M. Raimond, S. Haroche, and W. Gawlik, Phys. Rev. A **48**, 3991 (1993); S. Haroche, M. Brune, and J. M. Raimond, Europhys. Lett. **14**, 19 (1991).

[13] F. Yamaguchi, P. Milman, M. Brune, J. M. Raimond, and S. Haroche, Phys. Rev. A **66**, 010302(R) (2002).

[14] J. M. Raimond, M. Brune, and S. Haroche, Rev. Mod. Phys. **73**, 565 (2001).

[15] E. Hagley, X. Maître, G. Nogues, C. Wunderlich, M. Brune, J. M. Raimond, and S. Haroche, Phys. Rev. Lett. **79**, 1 (1997).

[16] D. Jaksch, J. I. Cirac, P. Zoller, S. L. Rolston, R. Côté, and M. D. Lukin, Phys. Rev. Lett. **85**, 2208 (2000).

[17] M. Saffman, J. Phys. B: At., Mol. Opt. Phys. **49**, 202001 (2016).

[18] S. Scheel and S. Y. Buhmann, Acta Phys. Slovaca **58**, 675 (2008).

[19] S. Y. Buhmann, *Dispersion Forces I: Macroscopic Quantum Electrodynamics and Ground-State Casimir, Casimir-Polder and van der Waals Forces* (Springer, Berlin, 2012).

[20] H. B. G. Casimir and D. Polder, Phys. Rev. **73**, 360 (1948).

[21] M. Donaire, M.-P. Gorza, A. Maury, R. Guérout, and A. Lambrecht, Europhys. Lett. **109**, 24003 (2015).

[22] M.-P. Gorza and M. Ducloy, Eur. Phys. J. D **40**, 343 (2006).

[23] J. M. Wylie and J. E. Sipe, Phys. Rev. A **30**, 1185 (1984); **32**, 2030 (1985).

[24] D. P. Craig and T. Thirunamachandran, *Molecular Quantum Electrodynamics* (Dover, New York, 1998).

[25] R. R. McLone and E. A. Power, Proc. R. Soc. London, Ser. A **286**, 573 (1965).

[26] E. A. Power and T. Thirunamachandran, Phys. Rev. A **51**, 3660 (1995).

[27] P. R. Berman, Phys. Rev. A **91**, 042127 (2015).

[28] M. Donaire, R. Guérout, and A. Lambrecht, Phys. Rev. Lett. **115**, 033201 (2015).

[29] P. Barcellona, R. Passante, L. Rizzuto, and S. Y. Buhmann, Phys. Rev. A **94**, 012705 (2016).

[30] P. W. Milonni and S. M. H. Rafsanjani, Phys. Rev. A **92**, 062711 (2015).

[31] F. London, Eur. Phys. J. A **63**, 245 (1930).

[32] S. B. Zheng and G. C. Guo, Phys. Rev. Lett. **85**, 2392 (2000); S. Osnaghi, P. Bertet, A. Auffeves, P. Maioli, M. Brune, J. M. Raimond, and S. Haroche, *ibid.* **87**, 037902 (2001).

[33] E. Urban, T. A. Johnson, T. Henage, L. Isenhower, D. D. Yavuz, T. G. Walker, and M. Saffman, Nat. Phys. **5**, 110 (2009); A. Gaëtan, Y. Miroshnychenko, T. Wilk, A. Chotia, M. Viteau, D. Comparat, P. Pillet, A. Browaeys, and P. Grangier, *ibid.* **5**, 115 (2009); T. Wilk, A. Gaëtan, C. Evellin, J. Wolters, Y. Miroshnychenko, P. Grangier, and A. Browaeys, Phys. Rev. Lett. **104**, 010502 (2010).

[34] L. Béguin, A. Vernier, R. Chicireanu, T. Lahaye, and A. Browaeys, Phys. Rev. Lett. **110**, 263201 (2013).

[35] J. J. Sakurai, *Advanced Quantum Mechanics* (Addison-Wesley, Reading, MA, 1994).

[36] J. D. Jackson, *Classical Electrodynamics* (John Wiley and Sons, New York, 1962).

[37] K. A. Milton, *The Casimir Effect: Physical Manifestations of Zero-point Energy* (World Scientific, Singapore, 2001).

[38] M. Donaire, Phys. Rev. A **93**, 052706 (2016).

[39] M. Donaire, Phys. Rev. A **94**, 062701 (2016).

[40] S. Y. Buhmann, L. Knoll, D. G. Welsch, and H. T. Dung, Phys. Rev. A **70**, 052117 (2004).

[41] S. Y. Buhmann, *Dispersion Forces II: Many-Body Effects, Excited Atoms, Finite Temperature and Quantum Friction* (Springer, New York, 2012).

[42] A. Reinhard, T. C. Liebisch, B. Knuffman, and G. Raithel, Phys. Rev. A **75**, 032712 (2007).

[43] J. Hare, Etude théorique et expérimentale des atomes de Rydberg circulaires: Vers une mesure directe de la constante de Rydberg en unités de fréquence, Ph.D. thesis, Universite Pierre et Marie Curie - Paris VI, 1991; Available online at https://tel.archives-ouvertes.fr/tel-00011877/.

[44] D. A. Steck, *Rubidium 87 D Line Data*, available online at http://steck.us/alkalidata (revision 2.0.1, 2 May 2008).

[45] P. R. Berman and B. Dubetsky, Phys. Rev. A **55**, 4060 (1997); P. W. Milonni and P. L. Knight, *ibid.* **10**, 1096 (1974).

[46] M. Donaire and A. Lambrecht, Phys. Rev. A **92**, 013838 (2015).

[47] A. Paris-Mandoki, H. Gorniaczyk, C. Tresp, I. Mirgorodskiy, and S. Hofferberth, J. Phys. B: At., Mol. Opt. Phys. **49**, 164001 (2016).

[48] S. Welte, B. Hacker, S. Daiss, S. Ritter, and G. Rempe, Phys. Rev. Lett. **118**, 210503 (2017).